PNEUMATIC PEANUT SKIN SLITTER

By

BETHEL JOE HERROLD

Bachelor of Science

Oklahoma State University

Stillwater, Oklahoma

1970

Submitted to the Faculty of the Graduate College
of the Oklahoma State University
in partial fulfillment of the requirements
for the Degree of
MASTER OF SCIENCE
May, 1974

PNEUMATIC PEANUT SKIN SLITTER

Thesis Approved:

Bobby F. Clary
Thesis Adviser

Gerald Brusewitz

Charles E Rice

N N Durham
Dean of the Graduate College

ACKNOWLEDGEMENTS

The research reported in this study was supported by funds from the Oklahoma Agricultural Experimental Station. This financial support is sincerely appreciated.

I am grateful to Professor E. W. Schroeder and Dr. Bobby L. Clary for securing funds and equipment and for providing facilities for this research. I also appreciate the financial assistance received from my assistantship in Agricultural Engineering.

I want to thank my major adviser, Dr. Bobby L. Clary, for his assistance and guidance during my graduate program. His availability for consultations was especially appreciated.

Appreciation is extended to Mr. Clyde Skoch and Mr. Norvil Cole for their assistance in constructing and setting up equipment in the Agricultural Engineering Research Laboratory.

To Mr. Jack Fryrear, I want to express my thanks for assistance in taking photographs and preparing figures used in this thesis. I would also like to thank Mrs. Sharon Hair for typing the final copy of this thesis.

I wish to thank Mr. Ronnie Morgan and Ms. LaDonna Moore for their endless time spent in preparing and separating the test samples.

To all my fellow graduate students, who have endured with me in my moments of despair, I am sincerely grateful.

I wish to dedicate this thesis to my wife, Margie, and daughter, JoDawna, for their devotion and sacrifices made during my graduate

program. I also want to thank Margie for her typing of the thesis draft.

TABLE OF CONTENTS

LIST OF TABLES

LIST OF FIGURES

CHAPTER I

INTRODUCTION

Background

Peanuts have long been an important factor in providing the world with a source of high protein food. Thus, the processing of peanuts has generated considerable interest recently. A large number of peanut products require blanching of the kernels early in the processing operation. Blanching in this context is defined as removal of the testa (or skin) from the peanut kernel, either before or after roasting.

The kernel testa has a bitter taste and imparts an undesirable flavor to processed peanut products. To insure consumer acceptance of processed products, such as peanut butter, candy, etc., manufacturers blanch kernels after roasting. This removes the skin and improves palatability of the manufactured food.

Color is another major factor in consumer acceptance of solvent-extracted meals and proteins processed from peanuts. Objectionable dark color in these products has been attributed to the presence of certain kinds of pigments in the skin. A majority of the peanuts produced in the United States are used for peanut butter. This is an industry of over 200 million dollars annually. Therefore, taste and color are important factors in determining peanut quality.

A third reason for blanching is the discovery of mycotoxin producing strains of fungi on peanut pods and kernels. With the discovery of

aflatoxin, a new interest has come about in developing processing techniques to insure that contaminated peanut products are not made available for human or livestock consumption. Removing skins from kernels can reduce contamination and reduce the difficulty in detecting contaminated kernels.

A technique is currently being investigated to remove the skins of non-contaminated and contaminated peanuts. Current techniques consist primarily of using peanut kernels below 9% moisture content, wet basis. The kernels are subjected to treatments that loosen the skin so it can be easily removed by the blancher. Satisfactory blanching has been obtained using heat, chemical and cryogenic treatments. Peanuts are blanched by moving the peanuts over abrasive rollers. Some peanut kernels have no flaws immediately evident in the skin and often pass through the abrasive blancher without having the skin removed.

A method is needed to effectively rupture the testa without damaging the kernel prior to blanching. Morgan (6) tested a slitter that mechanically moved each kernel between two knives where the testa was slit. Results of his tests indicated a pneumatic skin slitter would be possible in a blanching operation. An increase in production rate should also be achieved.

Objectives

Based on the results of Morgan (6) a skin slitter was designed and constructed to place three longitudinal slits 120 degrees apart on the surface of each peanut kernel. Specifically the objectives to this study were:

1. To design, construct and test a skin slitter using the Coanda

nozzle to convey kernels pneumatically through the slitter.

2. To determine effectiveness of the slitter in improving blanchability of raw Spanish peanut kernels.
3. To determine the effect of pneumatic conveying and slitting the skin on mechanical damage to the kernels.

CHAPTER II

REVIEW OF THE LITERATURE

Conventional Skin Slitter

Morgan (6) reported on the effects of initial peanut moisture content, force applied to the peanut kernel surface by the knife blade, and speed of the slitter disks of a conventional type peanut skin slitter. The effect of these variables on blanchability and mechanical damage was evaluated by a factorial experimental design. Initial moisture content was set at 7%, 8%, and 9%, slitter disks speed at 30 RPM, 60 RPM, and 100 RPM, and knife force at 90 grams, 170 grams, and 270 grams.

It is reported that slitter disks speed had no effect on either blanchability or percent whole kernels within the range of these tests.

An increase in blade force from 90 grams to 270 grams caused a significant increase in blanchability at 7% moisture content. The study showed that at 8% and 9% no effect of knife blade force on blanchability was found. It is also shown for 7%, 8%, and 9% initial moisture content there is a significant difference in percent whole kernels due to blade force. In each case, an increase in knife force caused a reduction in percent whole kernels. The effects of blade force were more pronounced as initial peanut moisture content increased.

Effects of moisture content on slit and nonslit testa showed that the effect of slitting the testa on blanchability was increased as

initial peanut moisture content was decreased from 9%. The difference between blanchability means was 15% at the lower initial moisture content and reduces to 5% at the higher initial moisture content. No effect on percent whole kernels was found when the testa was slit at 7% initial moisture content. However, as moisture content is increased to 8%, or 9%, differences between means of slit and nonslit treatments were significant.

The Coanda Nozzle

Reba (9) reported that a Romanian engineer, Henri Coanda, discovered a new phenomenon when he was experimentally testing a jet airplane he had designed. He was using deflecting plates to protect his fuselage from the flames. As he was making the take off run, he noticed with dismay that the deflecting plates, instead of diverting the exhaust away from the body of the plane, were actually sucking the flames toward it. Coanda took his discovery to Theodor von Karman who was working at the University of Gottingen. Von Karman said this was a new discovery and named it the Coanda effect.

Henri Coanda went on to make several devices, called Coanda nozzles, that utilized his discovery. The internal and external nozzles are the most common types. The internal nozzle (Figure 1) has the primary air chamber located around the nozzle opening. The external nozzle (Figure 2) has the primary air chamber located in the center of the nozzle with shrouding present to form the nozzle walls.

Everyone knows that it is difficult to pour a liquid smoothly out of a teapot spout or the mouth of a bottle. The liquid has an annoying tendency to flow around the lip and dribble down the curved surface of the spout or the side of the bottle. Water poured slowly from a glass

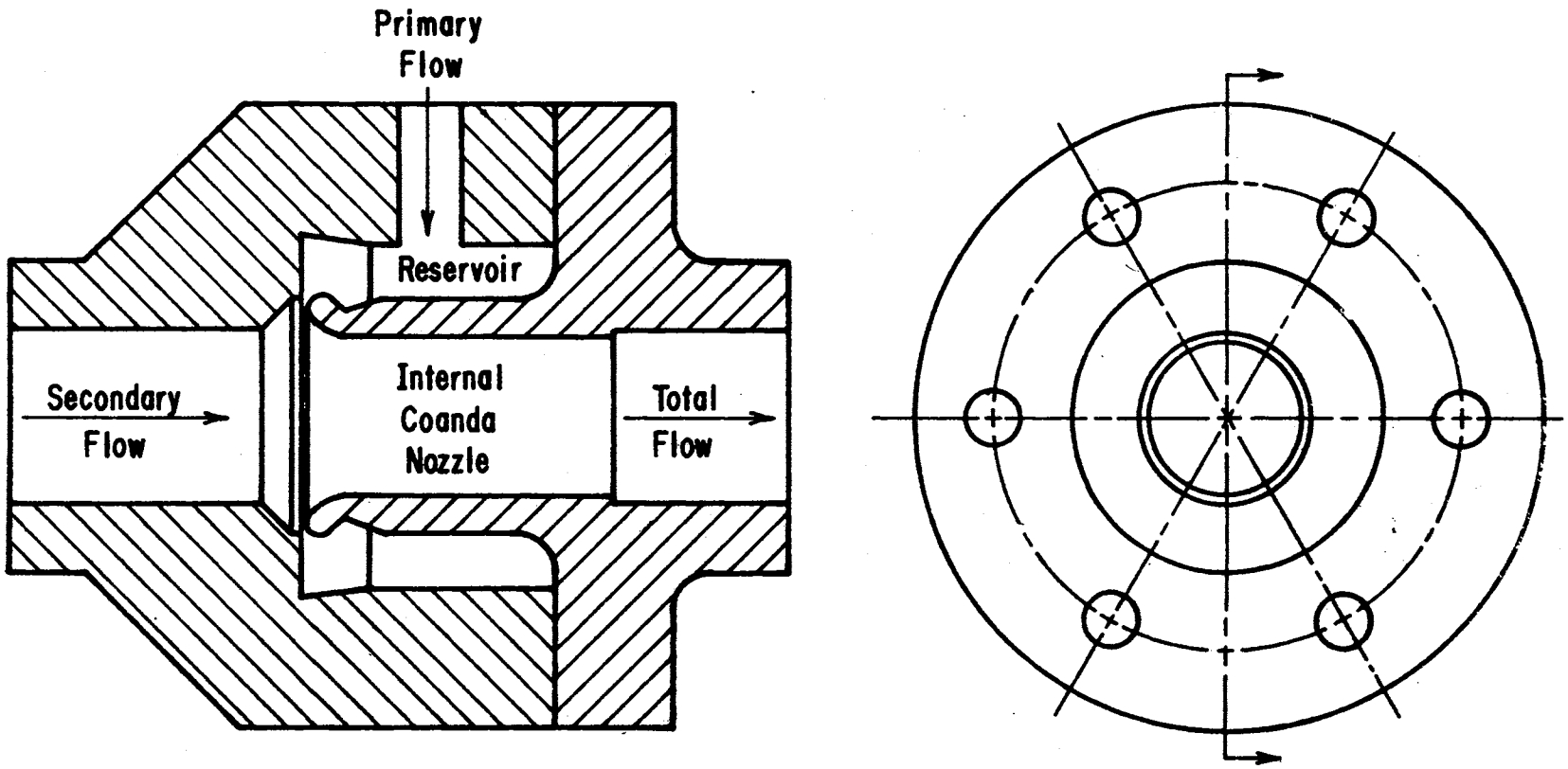

Figure 1. Internal Coanda Nozzle

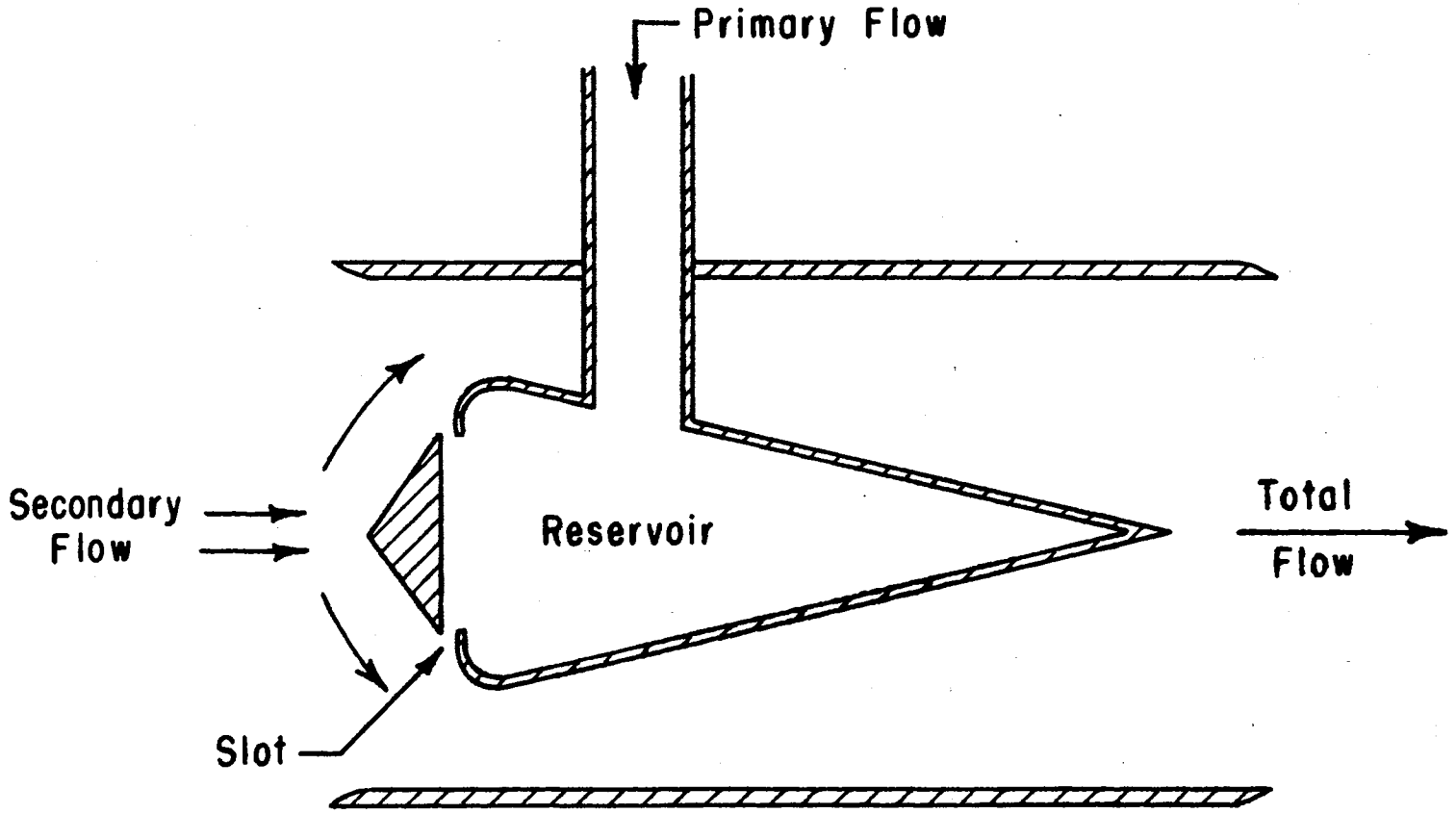

Figure 2. External Coanda Nozzle

tends to stick to the side of the glass in the same way that the tea sticks to the spout of a teapot. The "Teapot Effect" (9) is a low-speed form of the Coanda effect. High-speed fluids similarly adhere to a surface of suitable shape.

The Coanda effect causes a fluid to adhere to walls or to be deflected by a boundary in its path. The turning caused by the boundary and wall allows momentum and flow augmentation. Features of the Coanda nozzle are shown in Figure 1. The primary air flow enters the reservoir from outside sources and leaves the chamber through a slot, causing a high velocity air stream. This high velocity air entrains large quantities of ambient air in the nozzle. The fluid that is entrained near the deflection surface, which is called the secondary air stream, is accelerated causing a reduction in the static pressure on the surface. The lower pressure causes the jet stream to deflect toward the lower pressure and as a result, the jet stream is able to turn through a large angle and follow the deflecting surface.

Victory (13) ran and reported on a series of tests conducted on Dr. Henri Coanda's 70/84 type nozzle. The nozzle had a 7.0 centimeter throat diameter and a 66.8 centimeter divergent section following the nozzle. The slot opening was varied from 0.15 millimeter to 0.60 millimeter in the tests. The test range for the primary air flow was about 32 CFM to 190 CFM at pressures ranging from 19.6 psia to 54.5 psia. To evaluate the performance of the nozzle, Victory had to analyze the fluid thrust and momentum augmentation of the nozzle. Thrust augmentation (measured thrust/primary momentum) of 1.25 was obtained using all slot widths. Flow augmentation (exit flow/measure primary flow) ranging up to 16 was reached with a 0.15 millimeter slot opening. Momentum augmentation (exit

momentum/primary momentum) of 1.71 was obtained using all slot openings.

Reba (10) reports on the use of Coanda nozzles in tests to determine the feasibility of mass transportation with the nozzles. The total length of the system was 78 feet. There were three nozzles, 1.5 inch throat diameter, placed in the system. One nozzle was at the entrance, one was in the middle, and one was two feet from the exit of the 1.5 inch diameter conveying tube. The slot openings were varied from 0.002 inch to 0.010 inch. The primary flow was held constant at 25.74 CFM for different slot openings resulting in different pressures. The conveyed materials used were table tennis balls (2.5 grams), water-filled table tennis balls (30 grams), three inch long cylinders (8.3 grams), and three inch long cylinders (165 grams), all with approximately 1.5 inch diameters.

The 2.5 gram table tennis ball reached a velocity of 820 feet per second, when all three nozzles of the system were used, while the 165 gram cylinder only reached a velocity of 180 feet per second at the end of the system. The cylinder did not reach a terminal velocity as it was still accelerating when it reached the end of the system.

Wetmore (14) reported on a Coanda nozzle used for conveying feed grains. The nozzle had a one inch throat diameter. The slot opening was varied from 0.006 to 0.02 inches. The primary air flow rate was varied between 15 and 22 CFM. The conveying tube was one inch conduit aluminum pipe 58 feet in length. The Coanda nozzle had an adequate Coanda effect to cause a high velocity secondary air flow. However, when the 58 feet of conveying pipe was linked with the nozzle, the greatly added pressure losses for the free air caused the secondary air flow to be lowered below the velocity required to convey materials

pneumatically. When conveying grain sorgham in 38 feet of horizontal pipe it was reported that 65% to 80% of the pressure losses were due to the air flow, with the remainder due to the material. The study also showed the maximum material flow rate was considerably lower than the capacities of the other one inch pneumatic conveying systems.

CHAPTER III

DESIGN AND CONSTRUCTION

Dimensional Analysis

The Buckingham Pi Therorem (7) states that the relationship among the physical quantities which fully characterize a physical system can be expressed in terms of dimensionless parameters. The number of independent and dimensionless parameters, called Pi terms, necessary to describe this system is equal to the number of physical quantities minus the rank of the dimensional matrix corresponding to the physical quantities. This relationship among physical quantities can be reduced to an expression of the form:

$$f_n(\pi_1, \pi_2, \pi_3, \ldots \pi_n) = 0 \qquad (1)$$

Restrictions placed on the Pi terms are that they be dimensionless and independent.

The variables listed in Table I are a list of pertinent non-redundant physical quantities describing the system for blanchability and mechanical damage. The units utilized in this study are also shown in Table I. There are 19 physical quantities describing each system and four dimensions describing the quantities. A dimensional matrix for the variables shows the rank of the matrix is four, indicating that four independent dimensions exist. Therefore, fifteen Pi terms are needed to describe each system. Blanchability and mechanical damage were the two dependent quantities and were the quantities to be determined.

TABLE I

PERTINENT VARIABLES

No.	Symbol	Quantity	Units
1	Q	Primary Air Flow	ft^3/sec
2	d	Diameter of nozzle	ft
3	r	Characteristic roughness of nozzle	ft
4	P	Characteristic dimension of kernel (diameter)	ft
5	R	Kernel surface roughness	ft
6	ρ_a	Density of air	lb_m/ft^3
7	μ	Viscosity of air	$lb_f sec/ft^2$
8	S	Slot width of nozzle	ft
9	C	Coanda lip surface	ft
10	g_c	Universal Gravitational Constant (32.18)	$\frac{lb_m ft}{lb_f sec^2}$
11	A	Peanut kernel flow rate	lb_m/sec
12	M	Initial peanut moisture content	%
13	ρ_p	Peanut kernel density (absolute)	lb_m/ft^3
14	X	Number of blades in slitter	———
15	H	Knife depth	ft
16	K	Knife blade force	lb_f
17	E	Slitter material roughness	ft
18	B	Blanchability	%
19	W	Mechanical damage	%
20	L	Tube length	ft

Table II lists the Pi terms that describe the system. In this study there were eight Pi terms held constant. They were π_1, π_2, π_3, π_4, π_5, π_8, π_{10}, and π_{13}. The experimental design for the study is tabulated in Table III.

Coanda Nozzle

The Coanda nozzle (Figure 3) was machined from aluminum in two parts. One part contains the Coanda surface (Appendix A) while the other part contains the wall which forms the slot between it and the Coanda surface. The outside dimensions of the completed Coanda nozzle were 2.5 inches long and 2.0 inches in diameter. The Coanda nozzle was machined so the conveying tubes could be slipped into place and fastened by set screws if necessary.

It was hypothesized that an appropriate velocity could be obtained with a Coanda nozzle to convey peanut kernels since the velocity of the jet stream depends primarily on the slot width in the Coanda nozzle. The conveying tube diameter was set at 0.5 inch inside diameter, so a Coanda nozzle had to be designed from a prototype discussed in the literature.

A sectional view of the 70/84 Coanda nozzle, designed by Dr. Henri Coanda, was scaled down from a 2.75 inch throat to a 0.5 inch throat. The dimensions were taken from a copy of the report from SFERI-Coanda (1) and Wetmore (14). Dimensional analysis indicates the length dimensions can be scaled down directly from the dimensions in the reports.

Pneumatic Control System

The pneumatic control system consisted of the primary air source,

TABLE II

PI GROUPS

No.	Pi Term	No.	Pi Term
π_1	$\frac{r}{d}$	π_9	M
		π_{10}	X
π_2	$\frac{p}{d}$	π_{11}	$\frac{Kd}{Q\mu}$
π_3	$\frac{R}{d}$	π_{12}	$\frac{H}{d}$
π_4	$\frac{S}{d}$	π_{13}	$\frac{E}{d}$
π_5	$\frac{C}{d}$	π_{14}	B
π_6	$\frac{Q\rho_a}{\mu g_c d}$	π_{15}	W
		π_{16}	$\frac{L}{d}$
π_7	$\frac{A}{\rho_p Q}$		
π_8	$\frac{\rho_p}{\rho_a}$		

TABLE III

EXPERIMENTAL DESIGN

B	W	$\frac{Q\rho_a}{\mu g_c d}$	$\frac{A}{\rho_p Q} \times 10^4$	M	$\frac{Kd}{Q\mu}$	$\frac{H}{d}$	$\frac{L}{d}$
Measure	Measure	4100 4850 5700 6500 7300 8100 8850 9650	7.64	7%	7566	0.250	40
Measure	Measure	7300	3.18 5.09 7.64 10.18 12.73 15.27	7%	7566	0.250	40
Measure	Measure	7300	7.64	6% 7% 8% 9%	7566	0.250	40
Measure	Measure	7300	7.64	7%	1891 3783 5674 7566 9458 11349	0.250	40
Measure	Measure	7300	7.64	7%	7566	0.125 0.187 0.250 0.312 0.375	40
Measure	Measure	7300	7.64	7%	7566	0.250	10 20 40 60

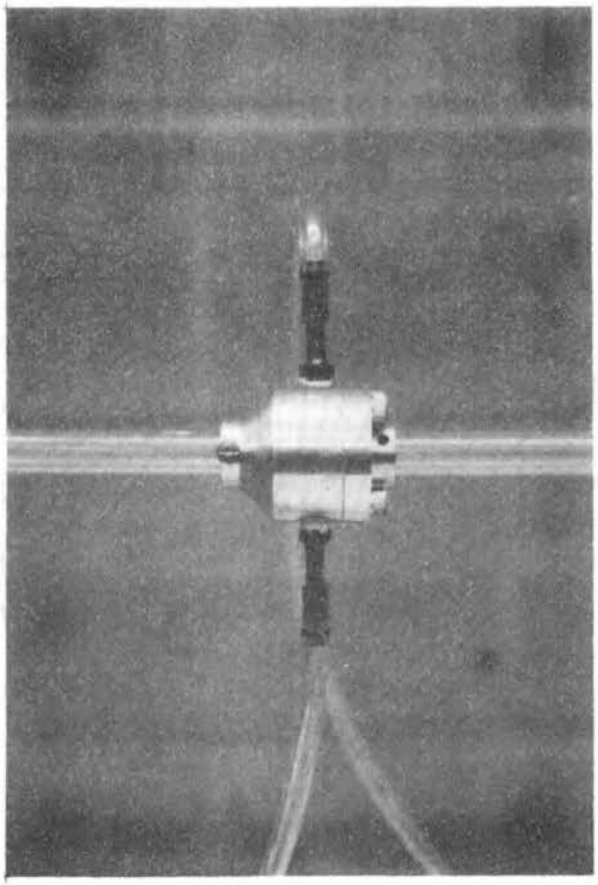

Figure 3. Coanda Nozzle

air volume and pressure controls, monitoring devices, secondary air tube, and pitot-static tube.

The laboratory air supply was used as the primary air source. A water trap was used to remove moisture from the air flow. A pressure regulator was used to control the primary air flow. A Fisher-Porter (No. 10A1735X4) rotameter measured the primary air flow into the nozzle. An 80 psi pressure gauge was mounted on the exit to the rotameter to give the approximate nozzle pressure. The primary air line consisted of two 0.25 inch plastic hoses which were connected to two sides of the Coanda nozzle.

For the secondary air path a 0.5 inch inside diameter plexiglass tube 15.50 inches was used. A 0.0625 inch pitot-static tube was mounted 6.75 inches upstream from the Coanda nozzle. The pitot tube was connected to a 25 centimeter U-tube manometer to measure the secondary air flow velocity head. From this secondary air flow was calculated. The pitot tube was removed when blanchability and mechanical damage tests were conducted.

Material Feeding Device

Figure 4 shows the vibrating kernel feeding system used to deliver peanut kernels to the secondary air tube. A HI-VI model V3B vibrated the 0.4 cubic foot aluminum hopper. Feed rates for the feeder system are shown in the experimental design (Table III).

Skin Slitter

The slitter block is shown in Figure 5. It was constructed from acrylic plastic rod four inches in diameter and a sheet of 0.25 inch acrylic plastic (plexiglass). Working drawings are shown in Appendix B.

Number 20 carbon steel surgical knives were mounted in a 1/4 x 1/4

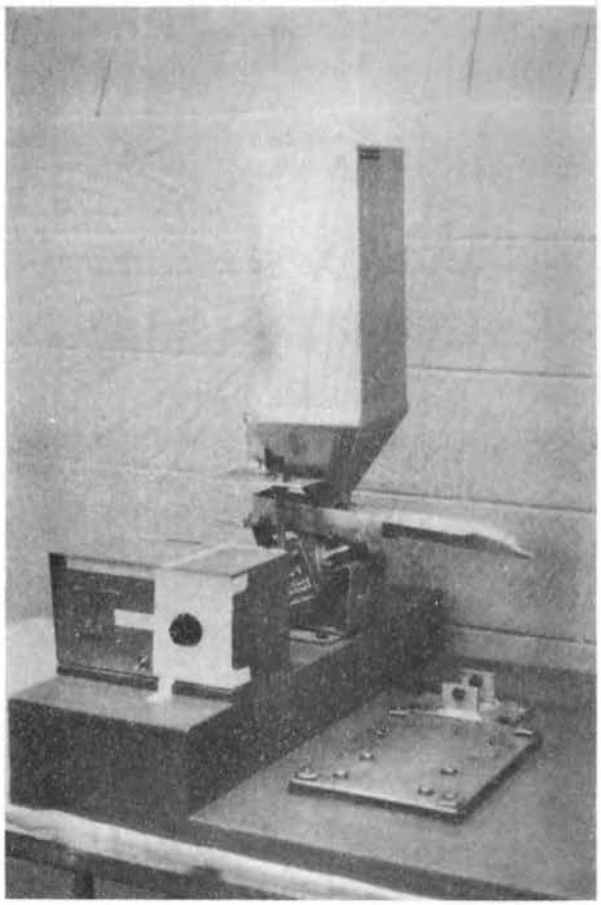

Figure 4. Vibration Feeder System

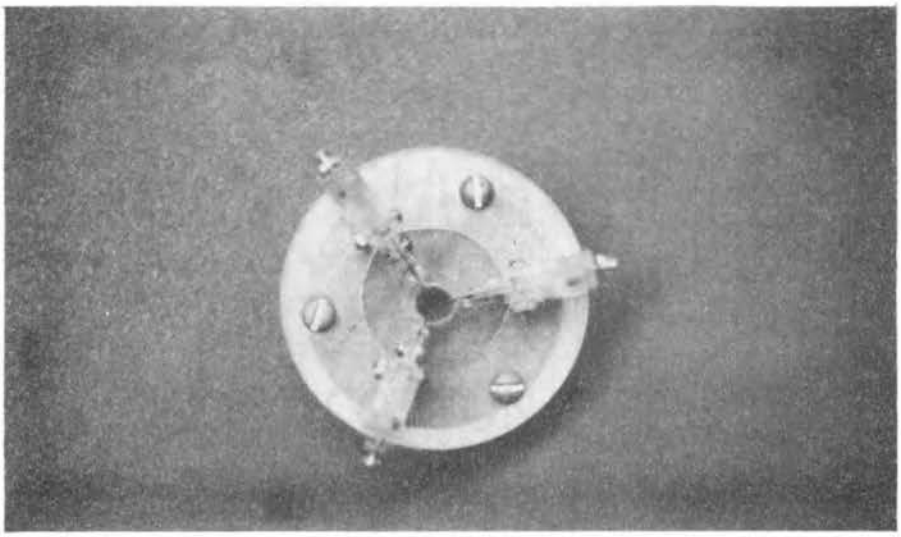

Figure 5. Slitter Block

x 2 inch piece of plexiglass to allow for easy replacement. Surgical blades were mounted 120° apart in the slitter block. Adjustable coil springs controlled tension on each knife.

The opening through the slitter block was 0.5 inch in diameter, the same as the tube through which the kernels travelled. A 0.637 inch hole was drilled in the front of the slitter block so the tube would fit securely.

Blancher

The blancher used was similar to the Ashton whole nut blancher (Figure 6). The blancher was constructed of aluminum and driven by a 1.25 hp. electric motor. The peanut kernels roll along two rotating rollers covered with abrasive surfaces. The rollers are 14 inches long and 2.5 inches in diameter. Roller speeds were 1060 rpm for the bottom roller and 1280 rpm for the top roller.

Dryer

A programmed laboratory dryer (Figure 7) was designed and constructed for heat treating peanut kernels. The dryer has a maximum temperature of 200°F. The dryer can control air temperature to $\pm$ 1°F. The drying unit can deliver 20 CFM per square foot.

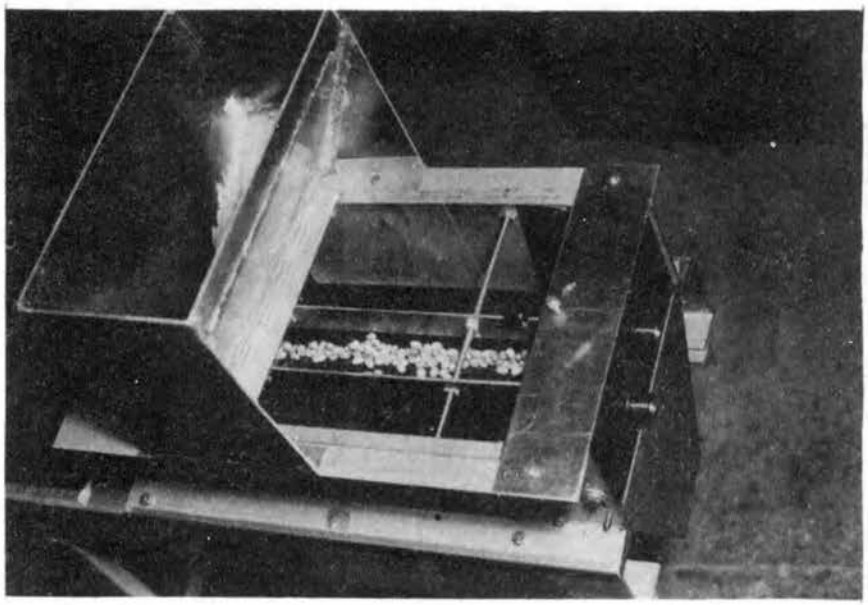

Figure 6. Whole Nut Blancher

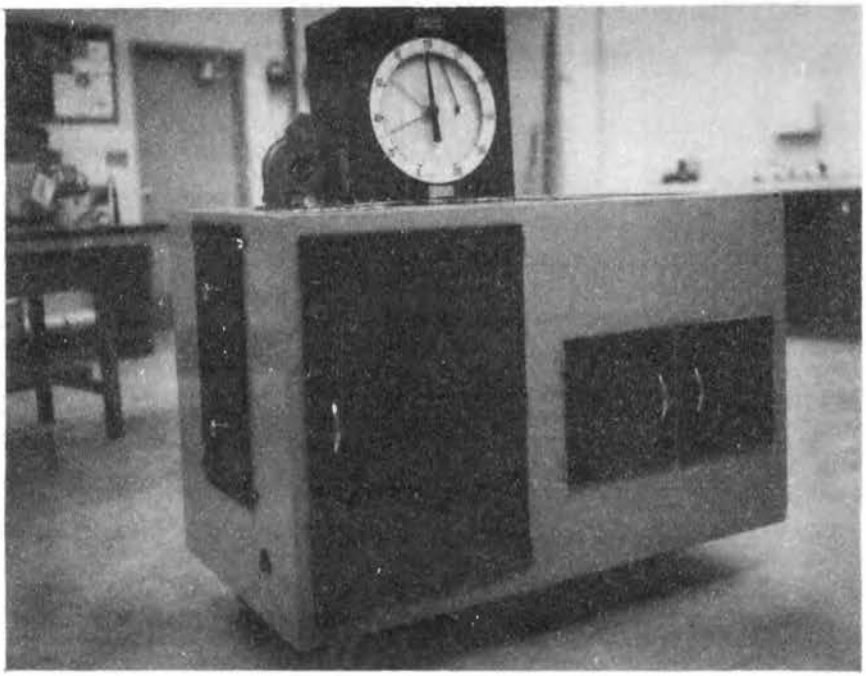

Figure 7. Laboratory Dryer

CHAPTER IV

EXPERIMENTAL PROCEDURE

Rotameter Calibration

The rotameter calibration curve is shown in Figure 8. From this curve the primary air flow was obtained. A linear scale from 0 to 1.5 units was etched on the rotameter tube. To measure velocity of the air entering the rotameter a 0.0625 inch pitot-static tube was used. The pitot tube was mounted in a 3/4 inch black iron pipe 1.50 feet preceding the rotameter. The black iron pipe was 6.75 feet long. Velocity head of the air was measured with a 25 centimeter manometer.

To obtain the calibration curve, air flow rate was controlled by a pressure regulator to set the scale reading on the rotameter. For this study the working range was from 0 to 1.05 units on the scale. Velocity head was measured at scale increments of 0.05 units starting at 0.10. Measured air flows are shown in Appendix C. From the measured air flow rate (CFM) and the scale reading a least-squares linear regression equation was derived (Figure 8) from a Statistical Analysis Systems program. The equation had a R-squared value of 0.998 with a standard deviation of 0.198 CFM.

A velocity traverse was run on the 3/4 inch black iron pipe to determine the relationship between the center line velocity and the average air velocity in the pipe. The pipe was divided into four equal areas and the pitot tube positioned in the pipe with the use of a micrometer. Three different scale readings were used and the velocity

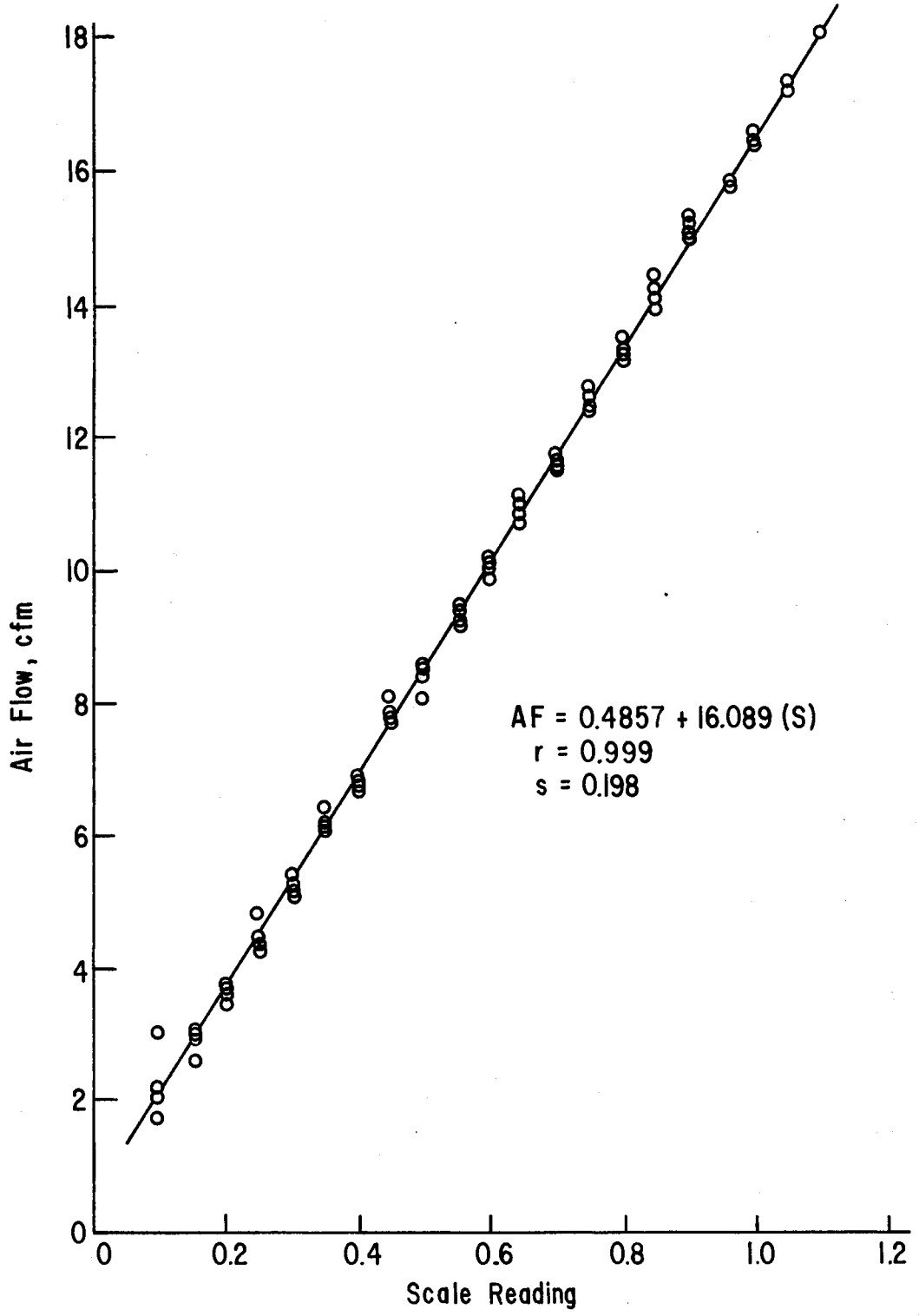

Figure 8. Air Flow for Rotameter Calibration

head measured at the centroid of the four area locations. This traverse showed the average velocity was 85 percent of the center line velocity.

Secondary Air Flow Rate Calibration

Secondary air flow rate was calculated from data taken from velocity head measurements. A 0.0625 inch pitot-static tube was located 8.75 inches from the secondary air inlet. Velocity head readings from the pitot tube were read on a 25 centimeter manometer.

Because there were four different lengths of tubes to be used between the nozzle and the slitter block, four different secondary air flow rates had to be established. Sixteen tests were conducted yielding four replications for each length of tube. These tests were run randomly. The data are recorded in Appendix C.

Peanut Speed Calculation

Speed of a peanut kernel travelling between the Coanda nozzle and the slitter block, in a half inch diameter plexiglass tube, was measured using photoelectric sensors. One sensor was placed at the exit of the nozzle and another sensor was located twenty-four inches downstream of the first sensor. These sensors were connected to a monitor and an oscilloscope. The oscilloscope had two channels, with one sensor connected to each channel.

A polaroid camera was mounted over the oscilloscope picture tube. By this means a black and white picture was taken of the trace as it traversed the scope. By setting the trace in different vertical locations on the scope it was possible to take seven pictures on one negative. Figure 9 shows examples of the pictures taken.

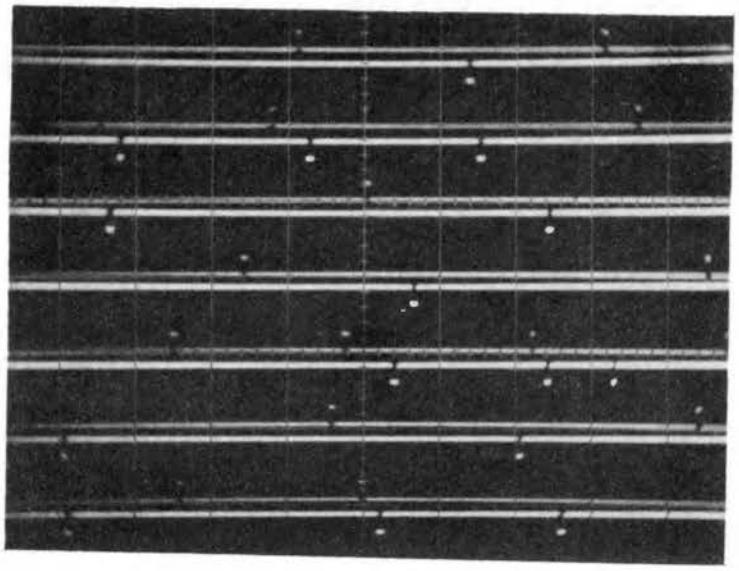

Figure 9. Picture of Trace for Kernel Velocity

The test procedure for the peanut kernel speed calculation with the above apparatus was as follows:

1. Turn power to the oscilloscope, monitor, and camera on.
2. Measure barometric pressure and conveying air temperature.
3. Set the desired primary air flow rate with the pressure regulator.
4. Set trace in desired location on oscilloscope tube.
5. Take picture of trace with kernel passing the sensors.
6. Steps four and five were repeated until seven traces were taken on each negative.
7. Steps three, four, five, and six were repeated until air flow rate was varied through the complete rotameter scale from 0.1 to 0.275 at 0.025 unit increments.

The above precedure was used on U. S. number one Spanish kernels. It was next used on U. S. number one Spanish kernels sized between eighteen sixty-fourths and nineteen sixty-fourths inch. Using a nineteen sixty-fourths inch standard sizing screen, U. S. number one Spanish kernels were placed on the screen and vibrated until all peanuts equal to or smaller than nineteen sixty-fourths inch were removed. All peanuts equal to or smaller than nineteen sixty-fourths inch were then vibrated on an eighteen sixty-fourths inch standard sizing screen to collect all peanuts larger than eighteen sixty-fourths inch.

Blanchability and Mechanical Damage

As discussed in Chapter III, the percent blanchability and mechanical damage were measured to evaluate the effects of the pneumatic skin slitter. To measure these two quantities, tests were randomly run as

shown in Table III.

For these tests U. S. number one Spanish kernels were purchased from a commerical supplier in southwest Oklahoma and stored at 40°F ± 2°F. The kernels were sorted to remove completely blanched and partially blanched kernels from test samples. Sorting was done by an ESM electronic peanut color sorter to remove the majority of blanched kernels. Remaining blanched kernels were manually removed. Moisture conditioning to 8% and 9% was accomplished by placing kernels in a controlled environmental chamber until the moisture content was hygroscopically increased to the desired level. These conditions could generally be reached within ten hours. Kernels were stored in air tight plastic bags to allow moisture equilibrium. After removal of blanched kernels, the unblanched kernels stored at 7% moisture content, were ready for testing. The 6% initial moisture was obtained by drying the kernels at 100°F ± 1°F in the dryer discussed earlier. After the desired moisture levels were obtained the kernels were separated into 500 gram samples and stored at 40°F ± 2°F until test time.

Tests were run according to the random number of the test. Peanut samples were removed from the cooler the night before the tests, allowing them to reach room temperature of 75°F ± 2°F. At the time of testing barometric pressure and air temperature were recorded. The desired values for the six Pi terms were set according to the random test. The initial moisture of the peanut sample was measured and recorded using a calibrated Steinlite Electronic Tester.

The peanut sample was placed into the vibratory feeder and skins were slit. As soon as the peanut skins were slit for the particular sample, it was placed in the laboratory dryer and dried at 160°F ± 1°F

to a final moisture of approximately 5%, wet basis. The test sample was allowed to cool to below 80°F. The final moisture content was determined and recorded. Next, the sample was placed into the whole nut blancher and the testa removed. Approximately the first 100 grams through the blancher were collected and discarded, as it was not typical of the blanched product (12). The remaining peanut sample was manually separated into blanched and unblanched samples. Any peanut kernel that was detected to have any testa still intact was said to be unblanched. Blanchability is the percent of peanut kernels by weight whose skin was totally removed by one pass through the blancher.

The blanched sample was further divided into samples of whole kernels and split kernels, those in which the cotyledons were separate. The whole and split samples were weighed and recorded.

Percent blanchability and percent whole kernels were calculated using equation 2 and equation 3.

$$B = \frac{100\ \beta}{\beta + \Psi} \tag{2}$$

$$W = \frac{100\ \phi}{\beta} \tag{3}$$

where,

B = blanchability, %

β = wt. of blanched kernels, gms.

Ψ = wt. of unblanched kernels, gms.

W = whole kernels, %

ϕ = wt. of whole blanched kernels, gms.

To determine effects of the pneumatic peanut skin slitter, several samples were run without using the slitter treatments. The results of these tests form a basis for determining the effectiveness of

slitting skins to increase the blanchability of raw Spanish peanut kernels.

CHAPTER V

PRESENTATION AND ANALYSIS OF DATA

Peanut Kernel Speed

The speed of the peanut kernels was calculated from data taken photographically as shown in Figure 9. The actual data are shown in Appendix C.

The distance was measured between the peanut kernel signals on each trace of the oscilloscope. This distance was multiplied by the time setting on the oscilloscope to yield the time it takes the peanut kernel to travel between the sensors, a distance of two feet. The distance divided by the time interval yields the velocity in feet per second.

Effects of the Reynolds number on kernel velocity is shown in Figure 10 for sized kernels and in Figure 11 for unsized kernels.

The graphs in Figure 10 and 11 show a large variation in kernel speed at a Reynolds number of approximately 9600. This Reynolds number is at the top of the working scale for this particular nozzle. The variation in kernel speed is caused by the Coanda nozzle not working properly when the trace was taken for some data points. The Coanda effect is broken by some kernels travelling through the system and then regained when another kernel passes through the nozzle.

Figure 12 shows the predicted regression lines for sized and unsized kernels. The sized kernels travelled with greater velocity

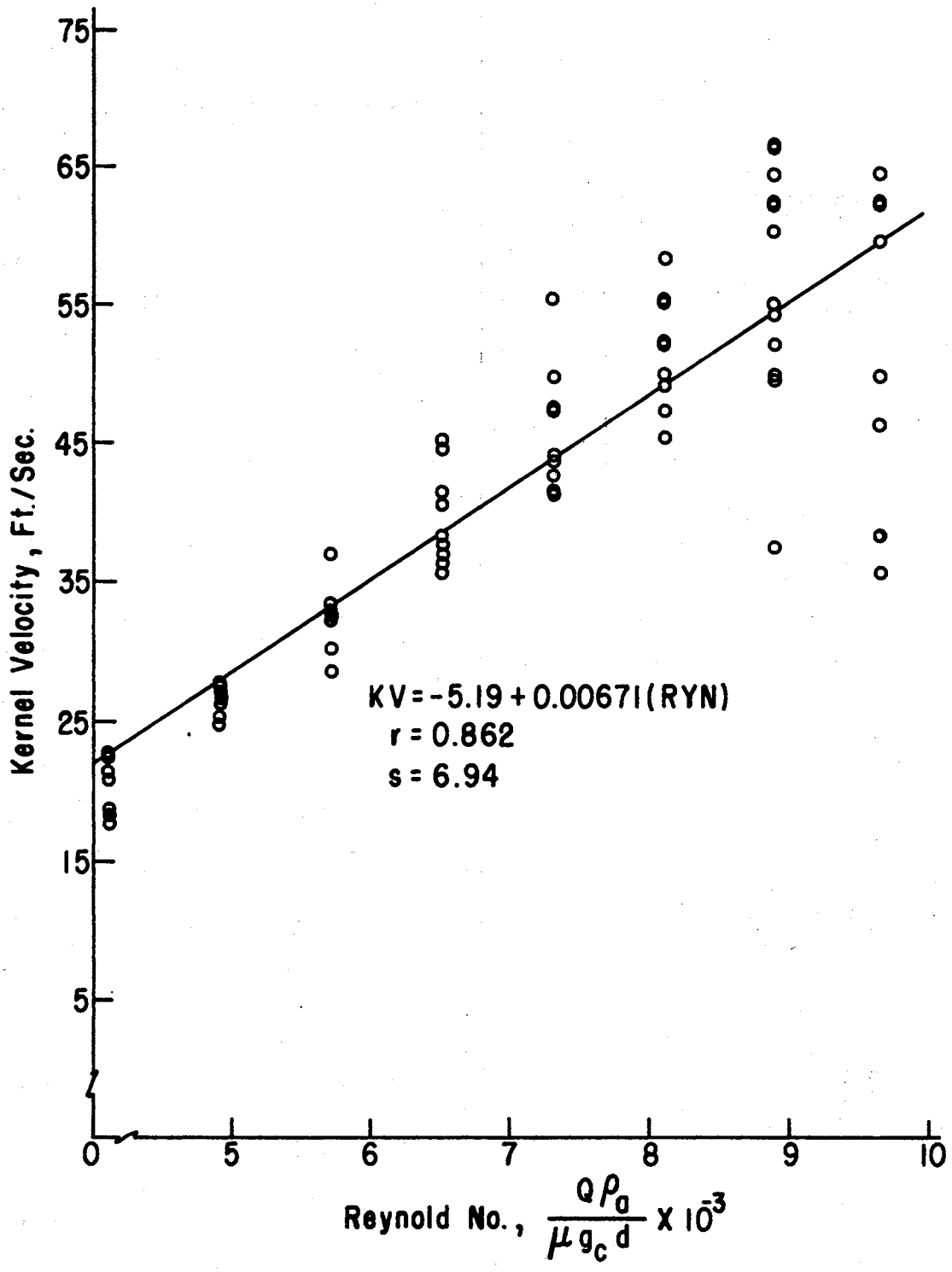

Figure 10. Kernel Velocity for Sized Peanut Kernels

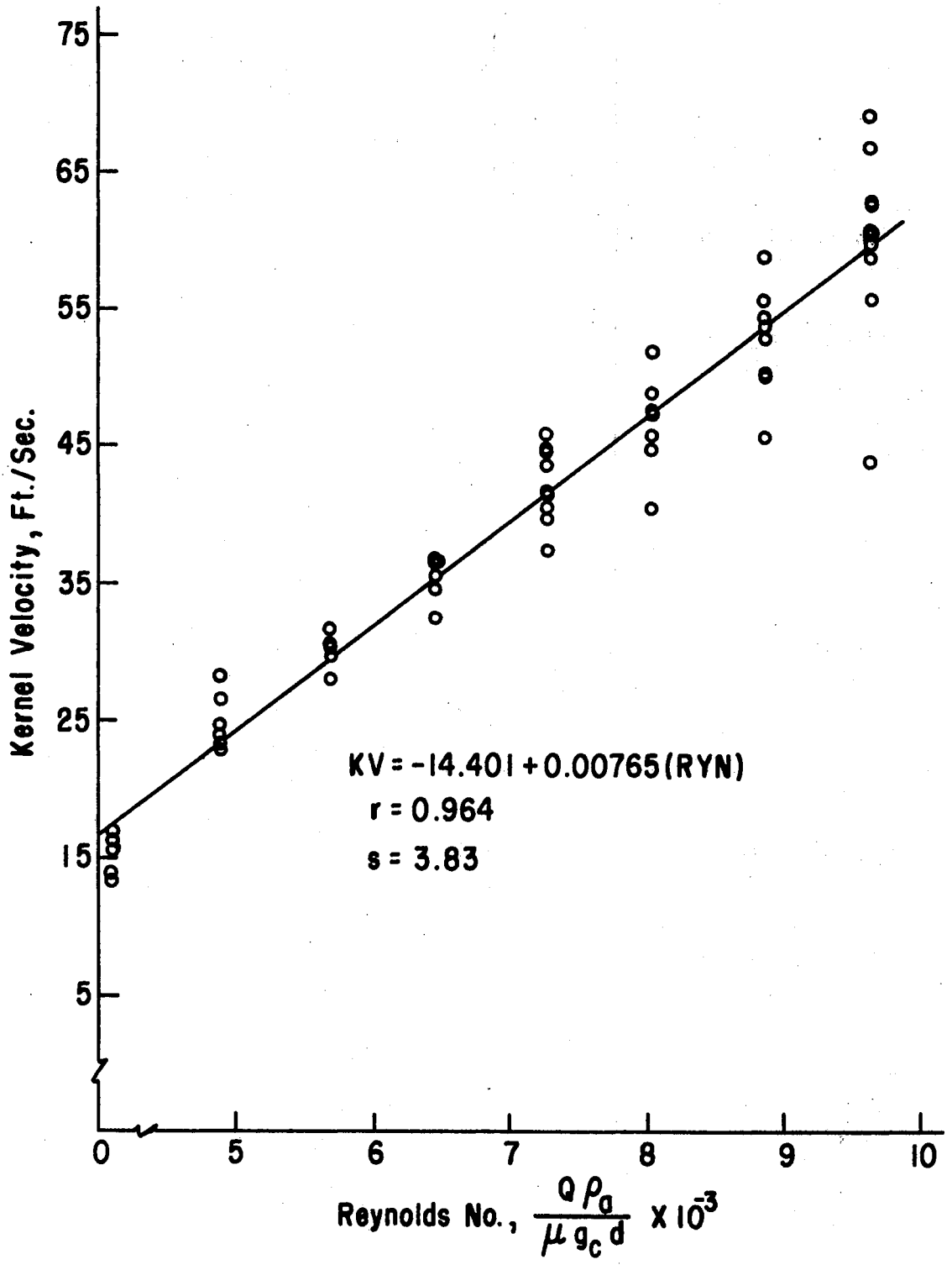

Figure 11. Kernel Velocity for Unsized Peanut Kernels

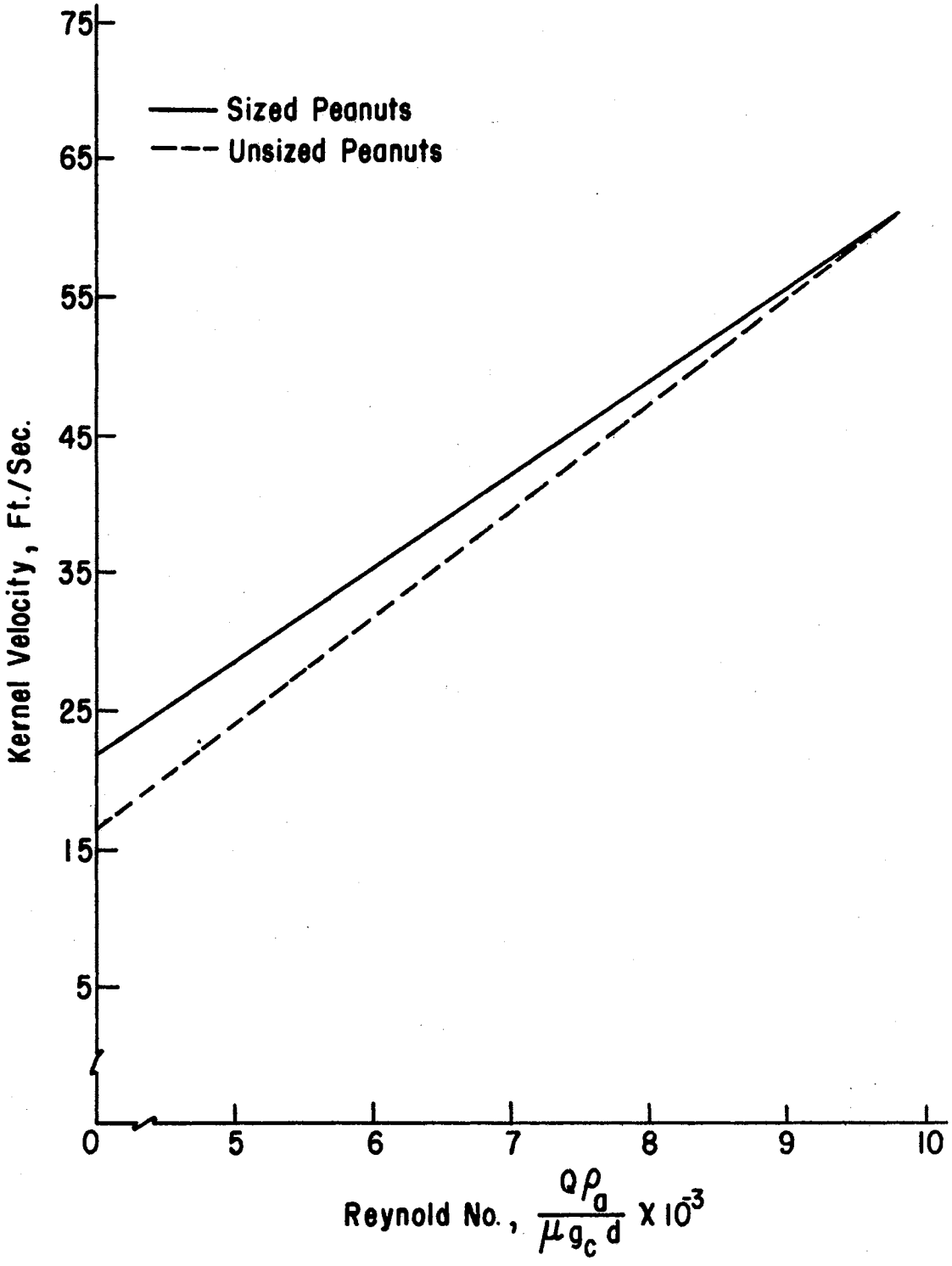

Figure 12. Comparison of Sized and Unsized Kernel Speed

until the higher Reynolds number, where the sized and unsized are practically the same.

Free Air Measurement With Different Tube Lengths

To determine the total air flow rate through the Coanda nozzle, new nozzle characteristics had to be determined. When shims were used in the Coanda nozzle to change the slot width, it was found that the Coanda effect was not created. Therefore, the slot width was not changed in any of the tests.

Air density was calculated using the equation in Marks (5) shown below.

$$D = \frac{B - 0.38P}{RT}$$

where

D = Air density, lb_m/ft^3

B = Barometric pressure, inches of Hg.

P = Vapor pressure of water, inches of Hg. at 32°F

R = Constant, 0.7541 inches of Hg.

T = Temperature, °R

Air temperature and barometric pressure were observed and recorded before each test. The vapor pressure was obtained from Table I in Marks (5).

Primary air flow rate was regulated in a rotameter scale range from 0.1 to 0.275 which represented 1.78 CFM to 4.17 CFM respectively. Four tests were run for each rotameter scale reading for the four different tube lengths.

Figures 13, 14, 15, and 16 show the data points and predicted

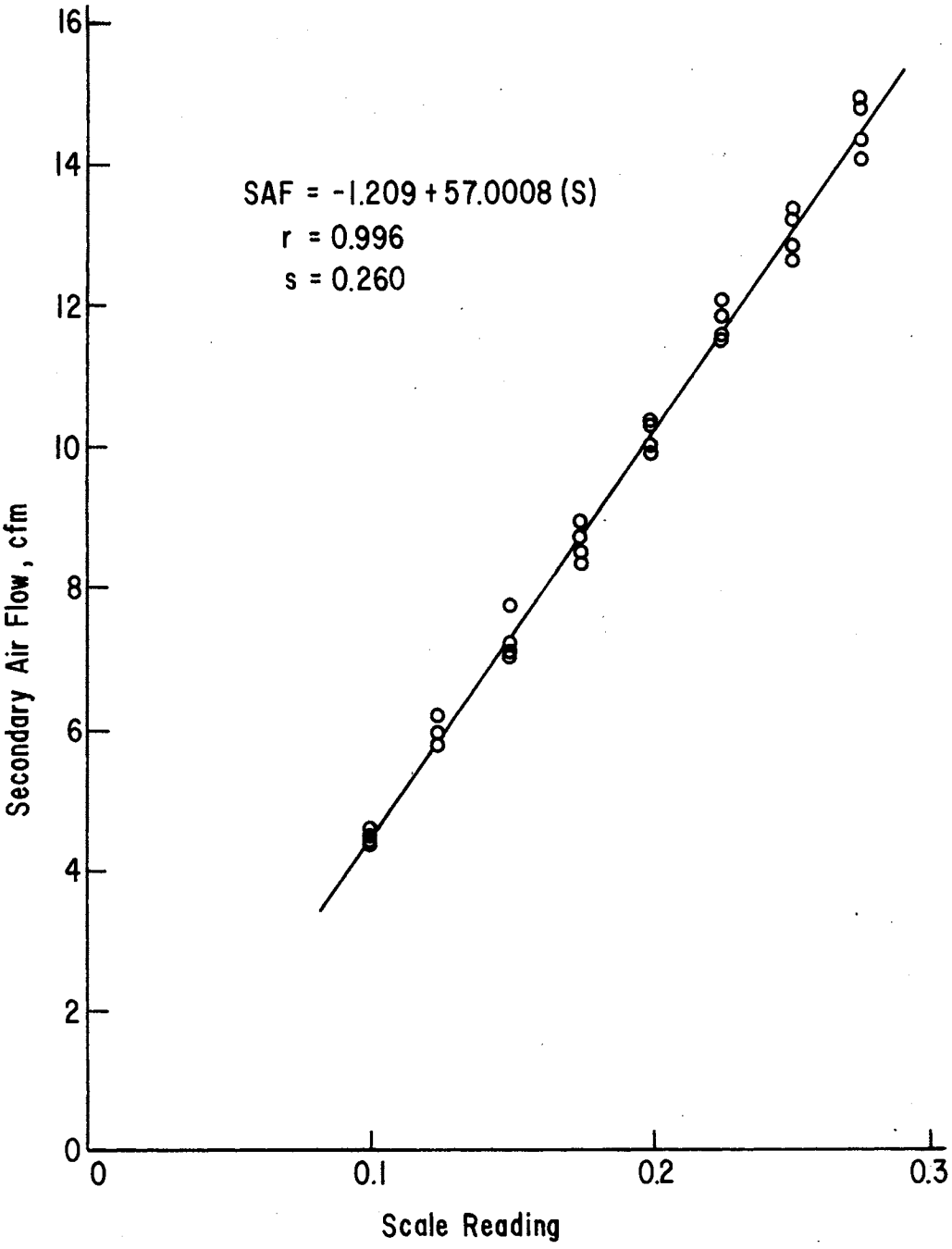

Figure 13. Secondary Air Flow for 5 inch Tube

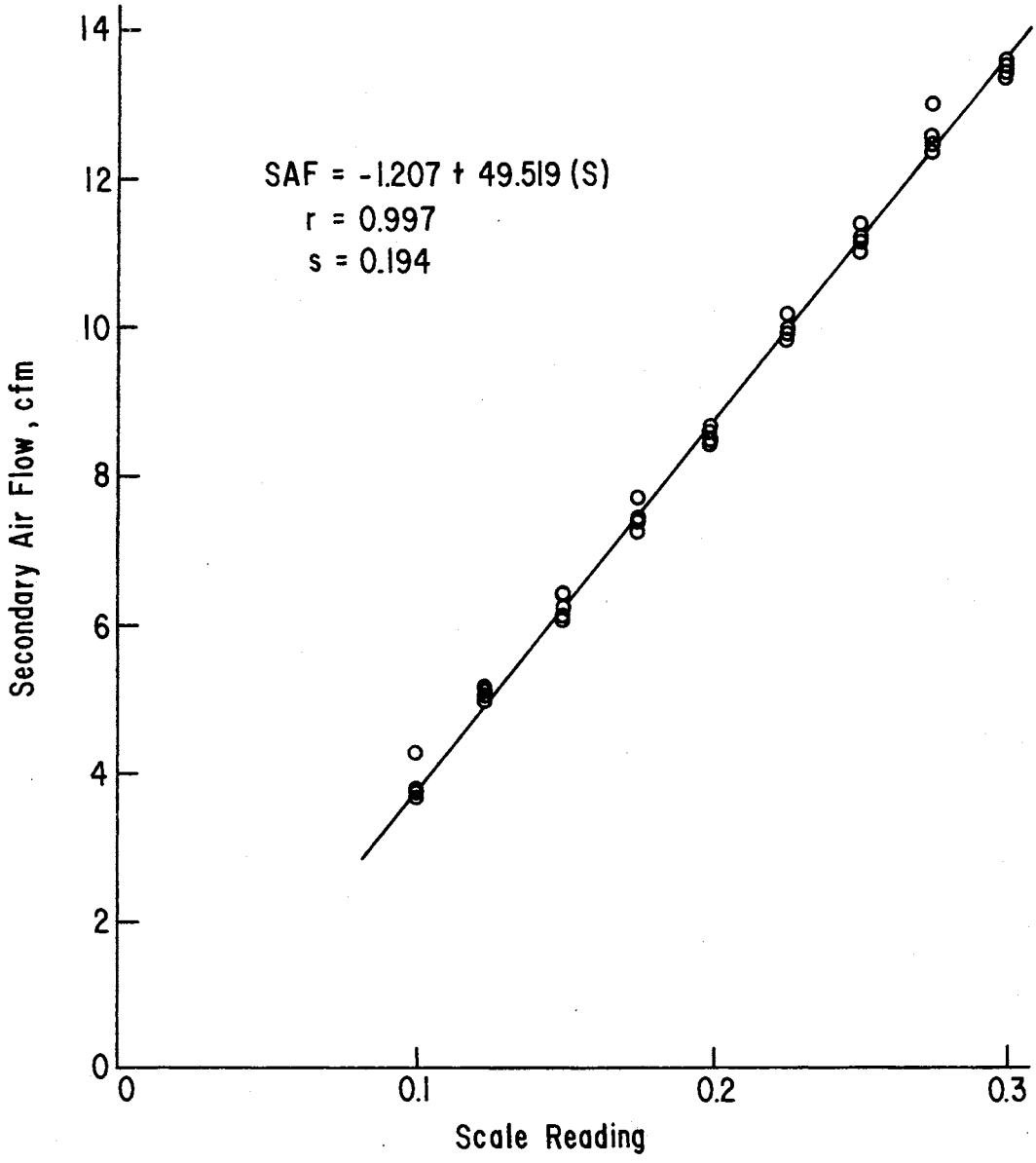

Figure 14. Secondary Air Flow for 10 inch Tube

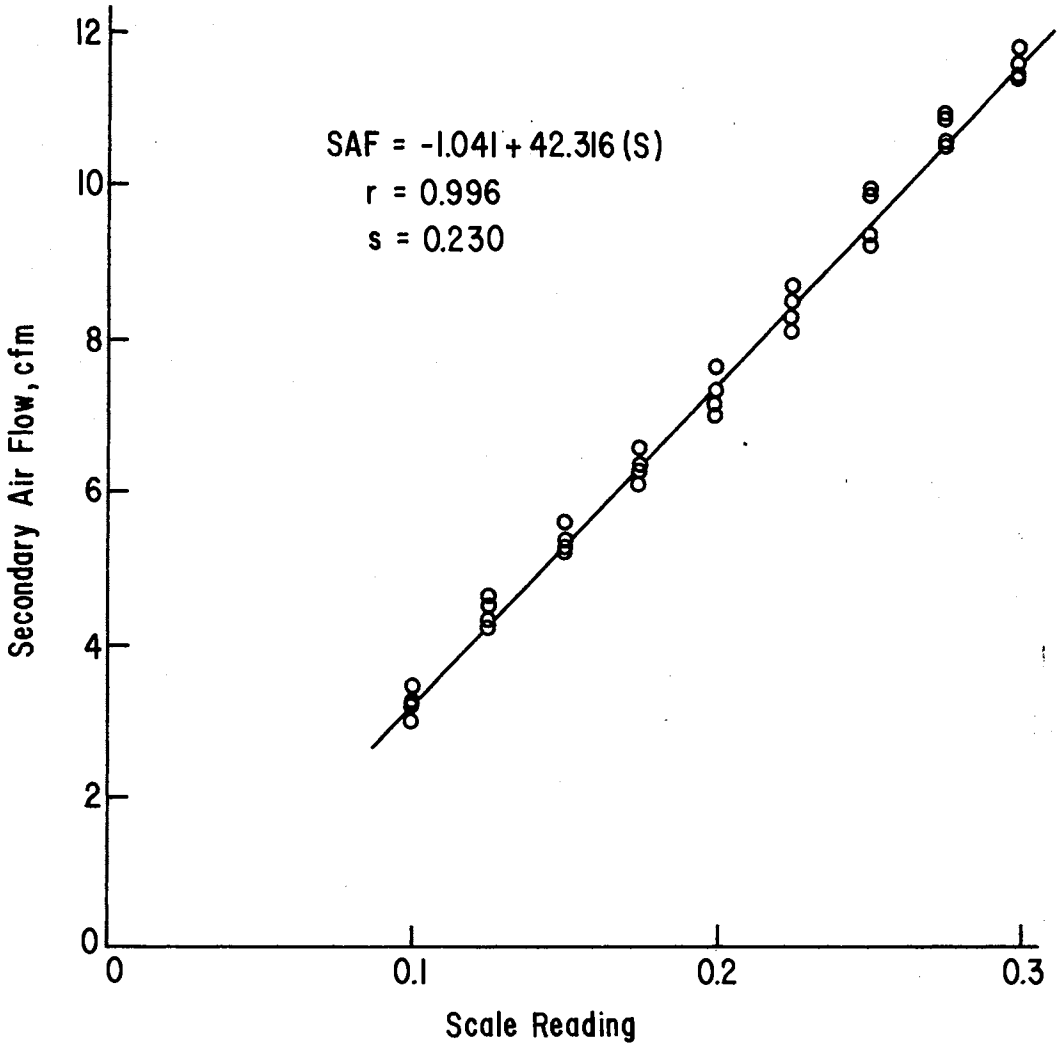

Figure 15. Secondary Air Flow for 20 inch Tube

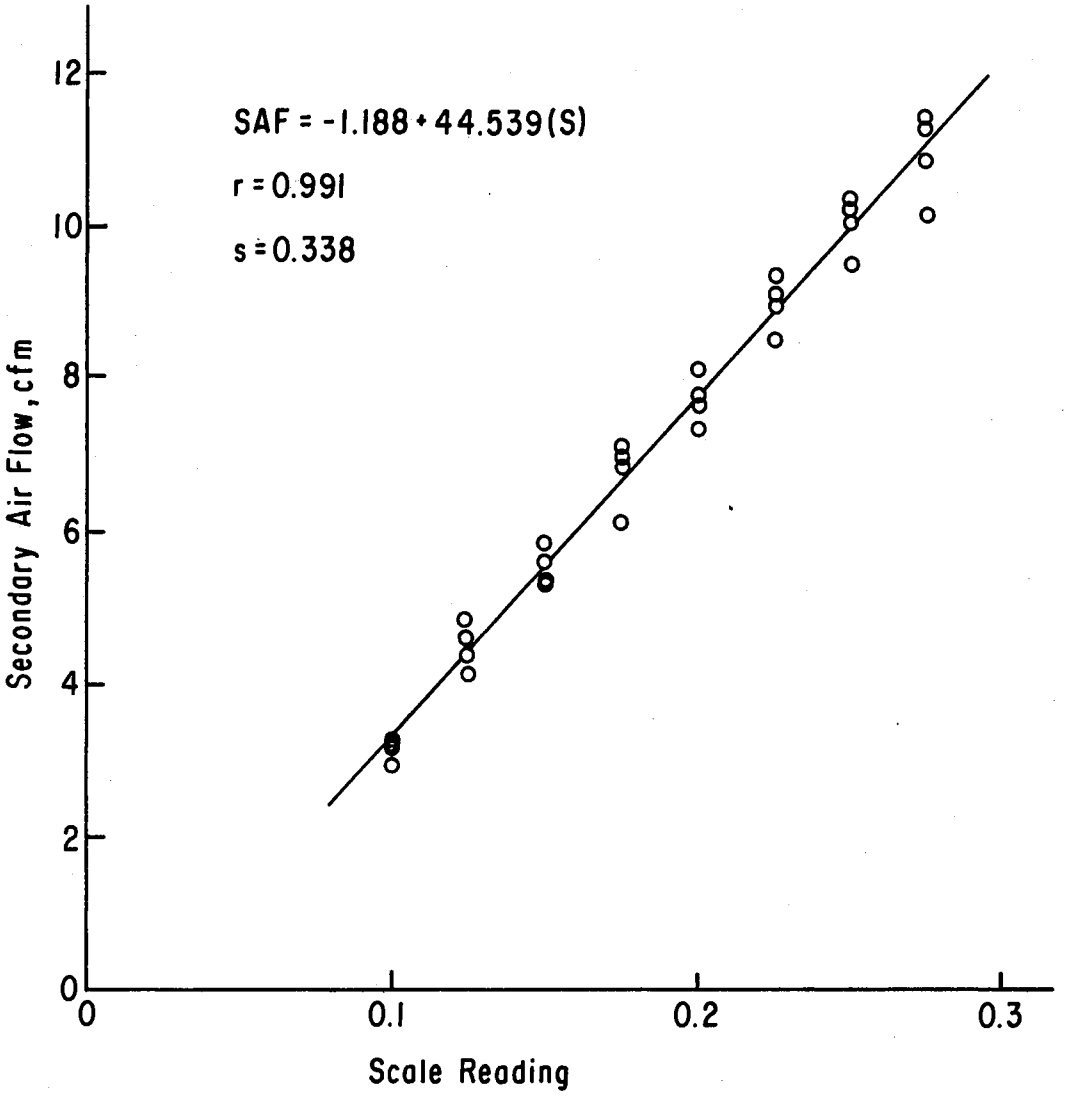

Figure 16. Secondary Air Flow for 30 inch Tube

regression equations plotted for the tube lengths, 5, 10, 20, and 30 inches, respectively.

Figure 17 compares secondary air flow rate as a function of tube length. It shows that the five inch tube has the greatest air flow rate of any length of tube. The twenty inch and thirty inch tubes are about equal.

Blanchability

A linear regression analysis was used to develop equations for blanchability as a function of the six Pi terms varied in the study. The analysis did not detect an effect on blanchability by three of the Pi terms. Figures 18, 19, and 20 show the data plotted for π_6 (Reynolds number), π_7 (feeder speed), and π_{16} (tube length), respectively. A horizontal line is drawn through the mean for each Pi term. Thus, the number of component equations for π_{14} is reduced to the three f_9, f_{11} and f_{12}.

Effects of π_{12}, blade depth term, on blanchability is shown in Figure 21. The F-test shows the slope of the line is different from zero at the 95% confidence level. The component equation for blade depth is

$$f_{12}\ (\bar{\pi}_9,\ \bar{\pi}_{11},\ \pi_{12}) = 83.61 + 15.78\ \pi_{12} \qquad (4)$$

As the blade depth is increased the blanchability also increases. At the 0.187 level of π_{12} two additional replications were run. This was done because of the dispersion of the first three replications at this point. This variation in blanchability is caused by the blades barely reaching into the travelling path of the kernel in the slitter. With the proper orientation some peanuts could pass the blades without being

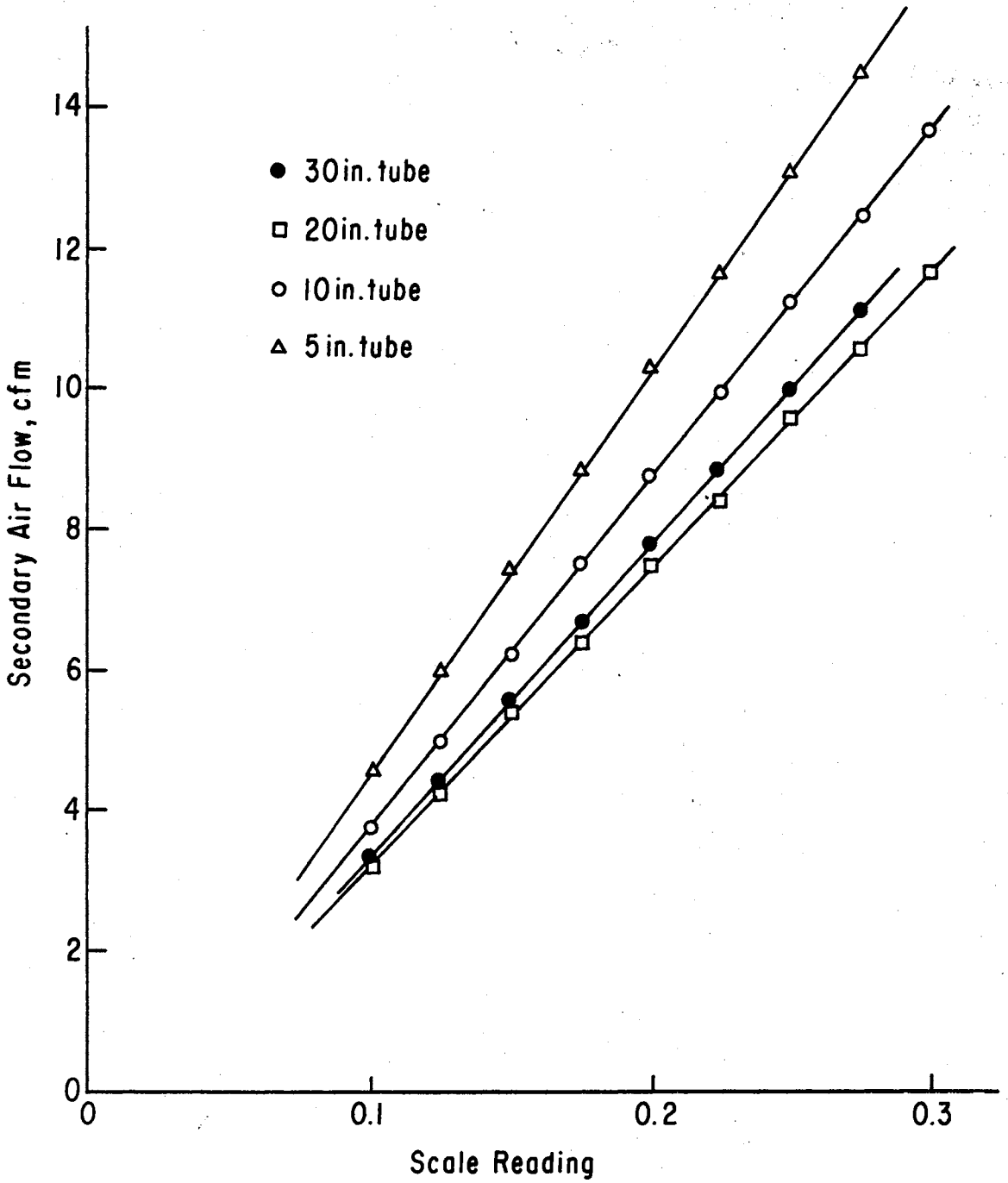

Figure 17. Comparison of Air Flows for Different Lengths of Tubes

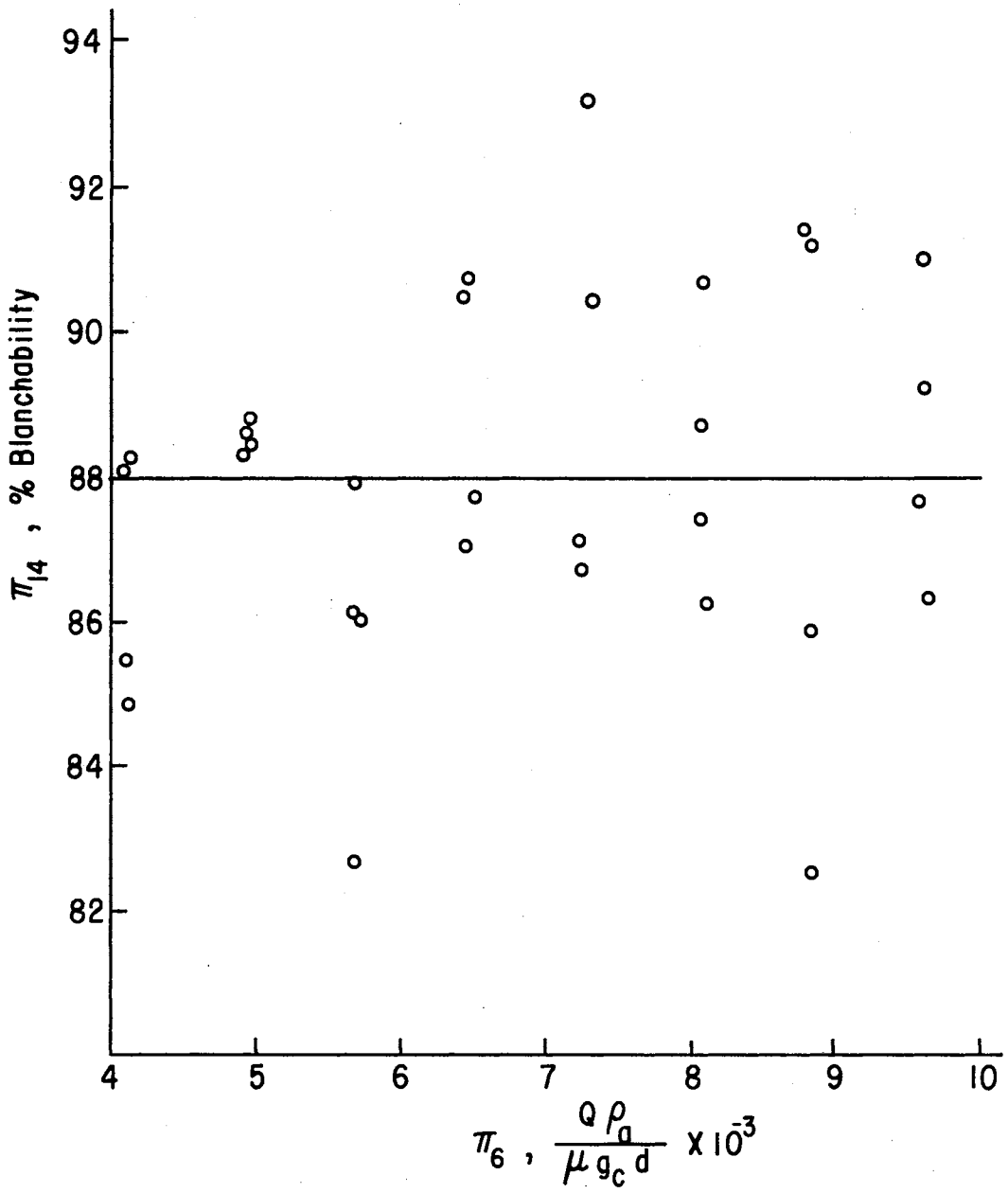

Figure 18. Effects of Reynolds Number on Blanchability

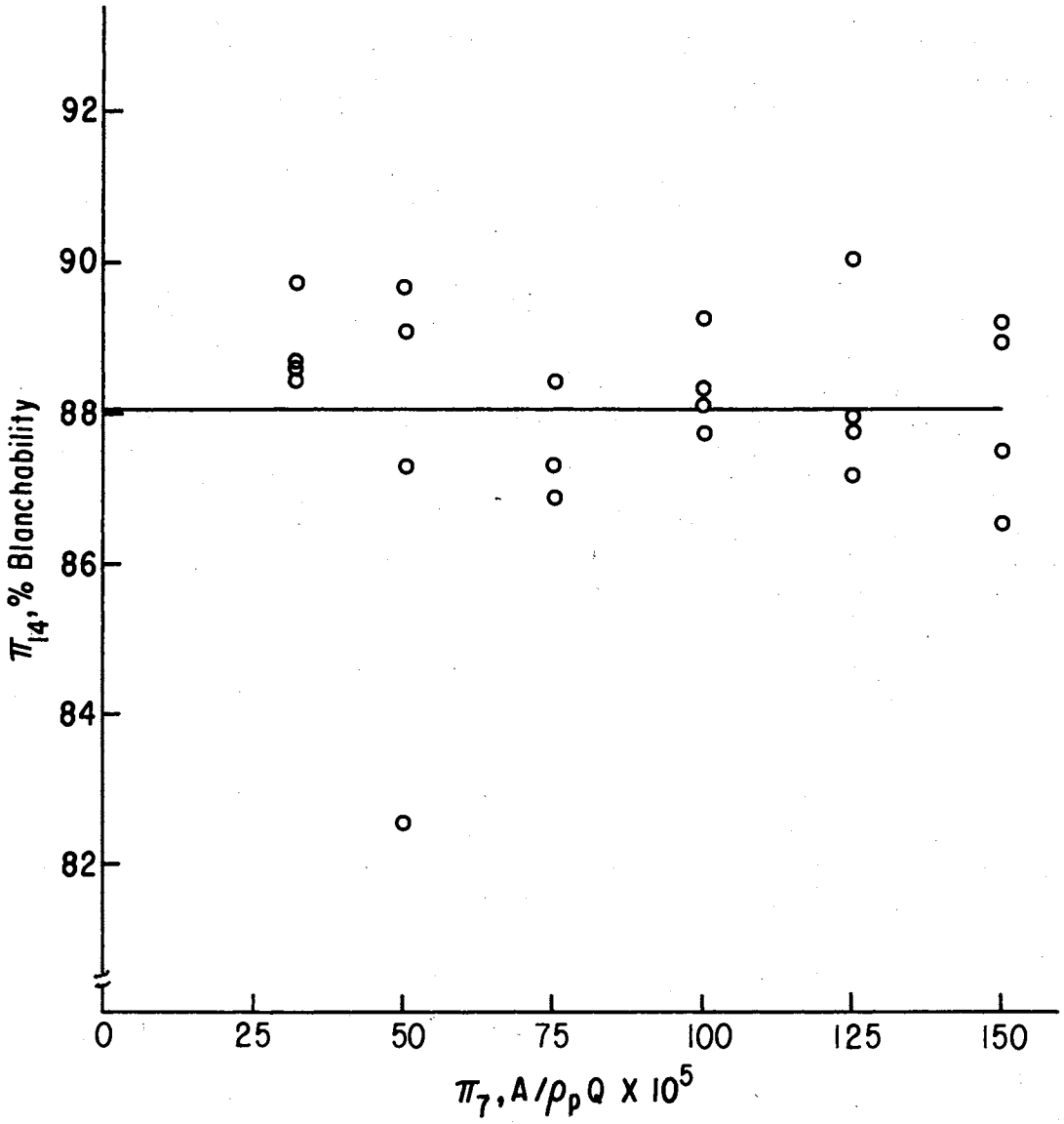

Figure 19. Effects of Feeder Speed on Blanchability

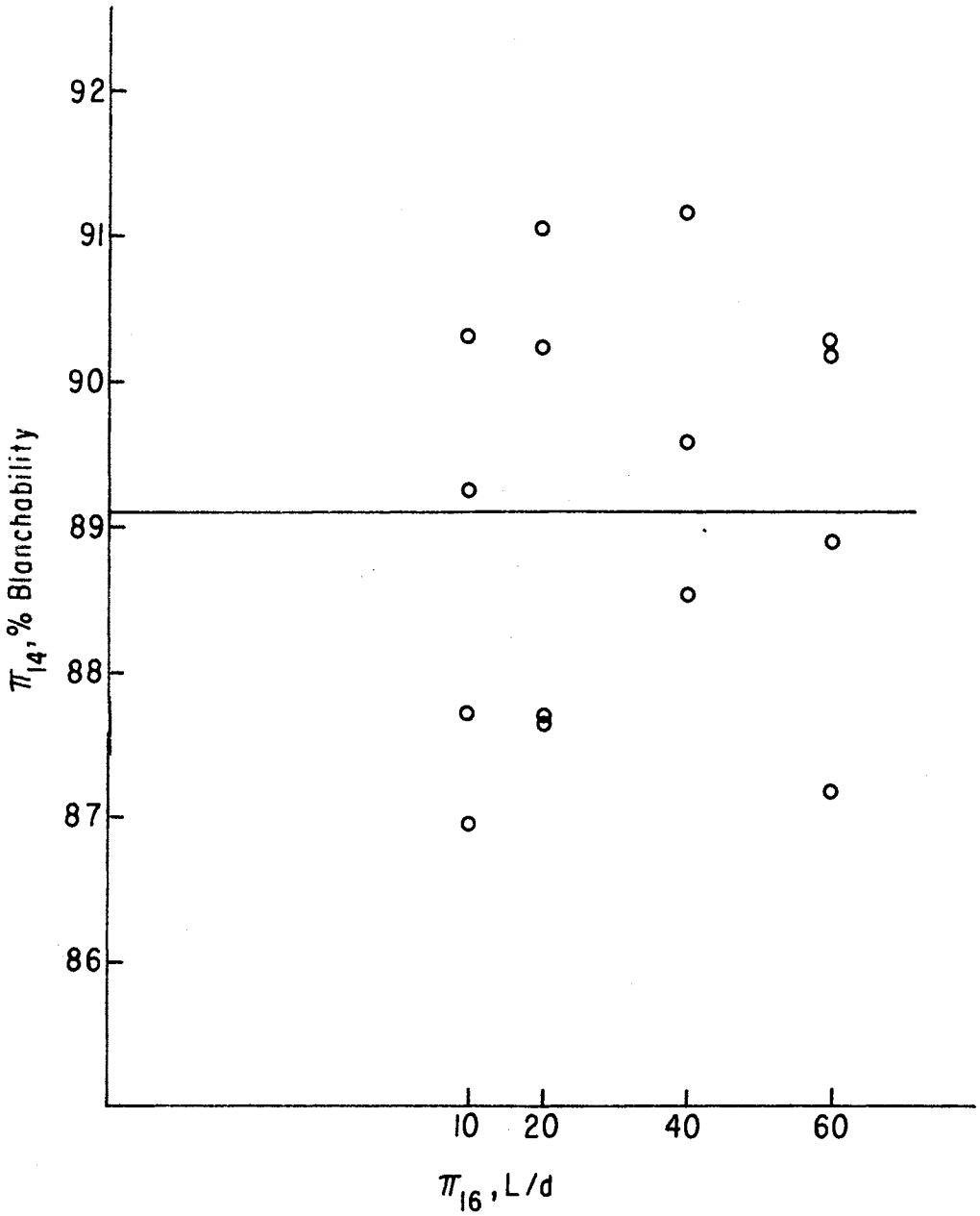

Figure 20. Effects of Tube Length on Blanchability

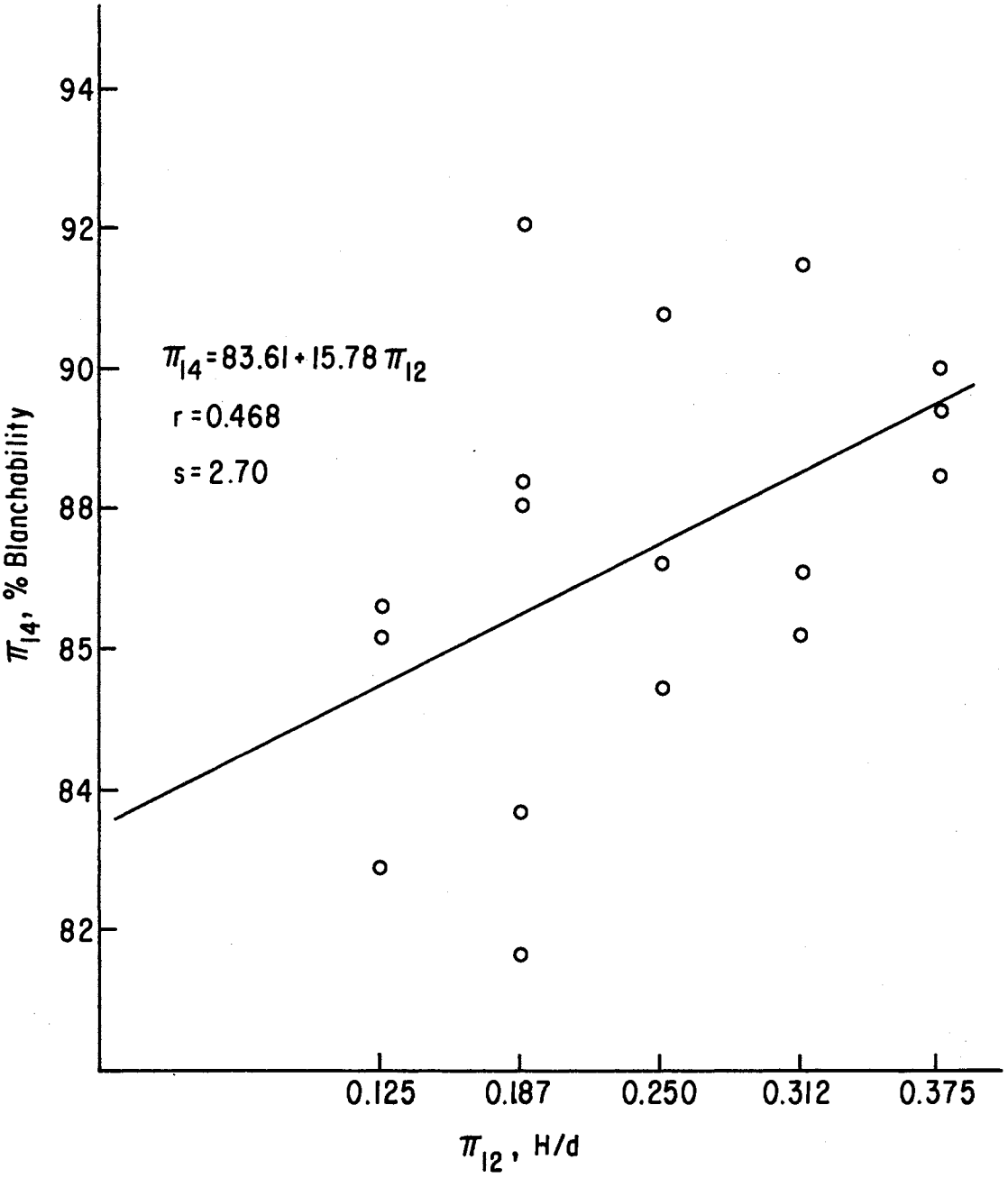

Figure 21. Effects of Blade Depth on Blanchability

slit, thus causing the low readings at this point. While in other samples a higher percentage of the kernels could be slit causing the higher readings.

Effects of π_9, initial moisture content, on blanchability, π_{14}, is shown in Figure 22. The regression line is different from zero at the 99.9% confidence level. The component equation for initial moisture content is

$$f_9 (\pi_9, \bar{\pi}_{11}, \bar{\pi}_{12}) = 76.32 + 1.82 \pi_9 \quad (5)$$

As the initial moisture content increases from 6% to 9%, blanchability increases about 5.5% due to slitting the kernels. Figure 23 shows the plotted data for nonslit tests. This regression line is different from zero at the 99.9% confidence level. By comparing Figure 22 and 23 the slittler effectiveness can be evaluated. At the initial moisture content of 6% there is a 5% increase in blanchability and at 9% initial moisture content there is a 1% increase in blanchability when the testa is slit prior to blanching.

Figure 24 shows the effect of π_{11}, blade force, on blanchability. The regression equation line is different from zero at the 95% confidence level. The component equation for blade force is

$$f_{11} (\bar{\pi}_9, \pi_{11}, \bar{\pi}_{12}) = 86.8 + 0.00021 \pi_{11} \quad (6)$$

As the blade force increases the blanchability also increases.

Mechanical Damage

A linear regression analysis was used to develop equations for mechanical damage as a function of the six Pi terms varied in the study. The effect of π_6, Reynolds number, on mechanical damage is shown in Figure 25. Calculation of the F-test statistic shows that the slope of the line generated is significantly different from zero at the 99.9% confidence level. The component equation for Reynolds number is

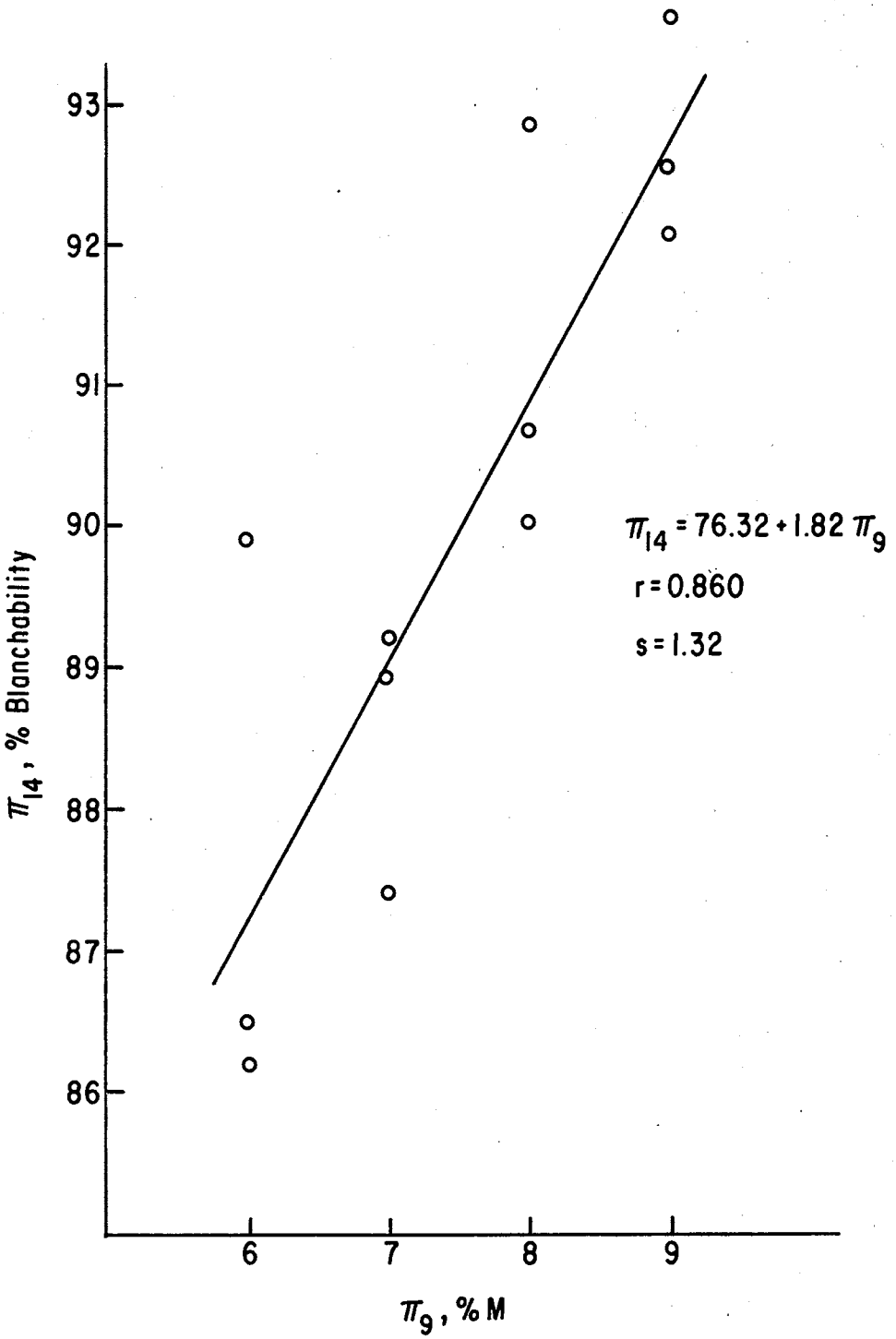

Figure 22. Effects of Initial Moisture Content of Slit Testa on Blanchability

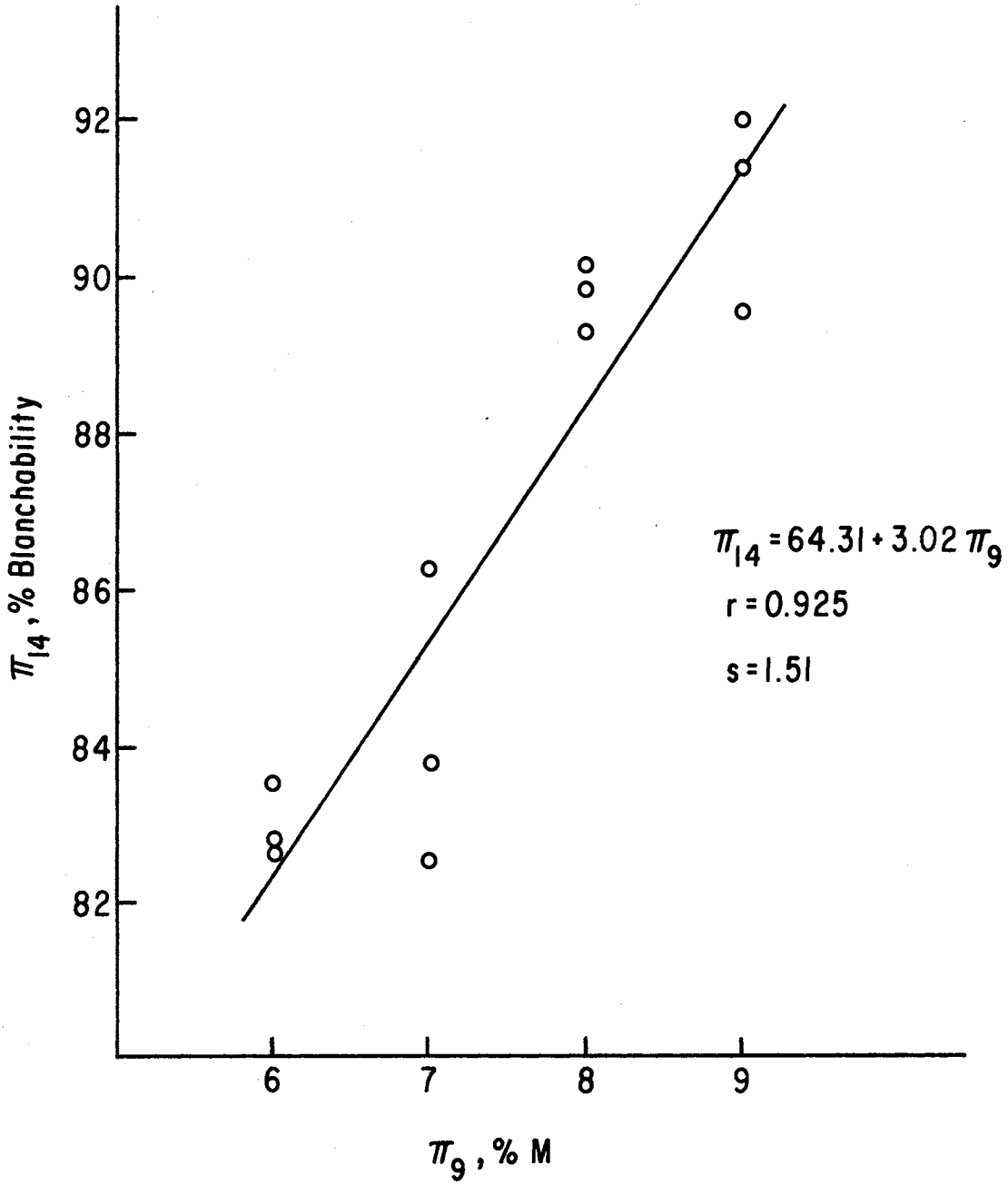

Figure 23. Effects of Initial Moisture Content of Nonslit Testa on Blanchability

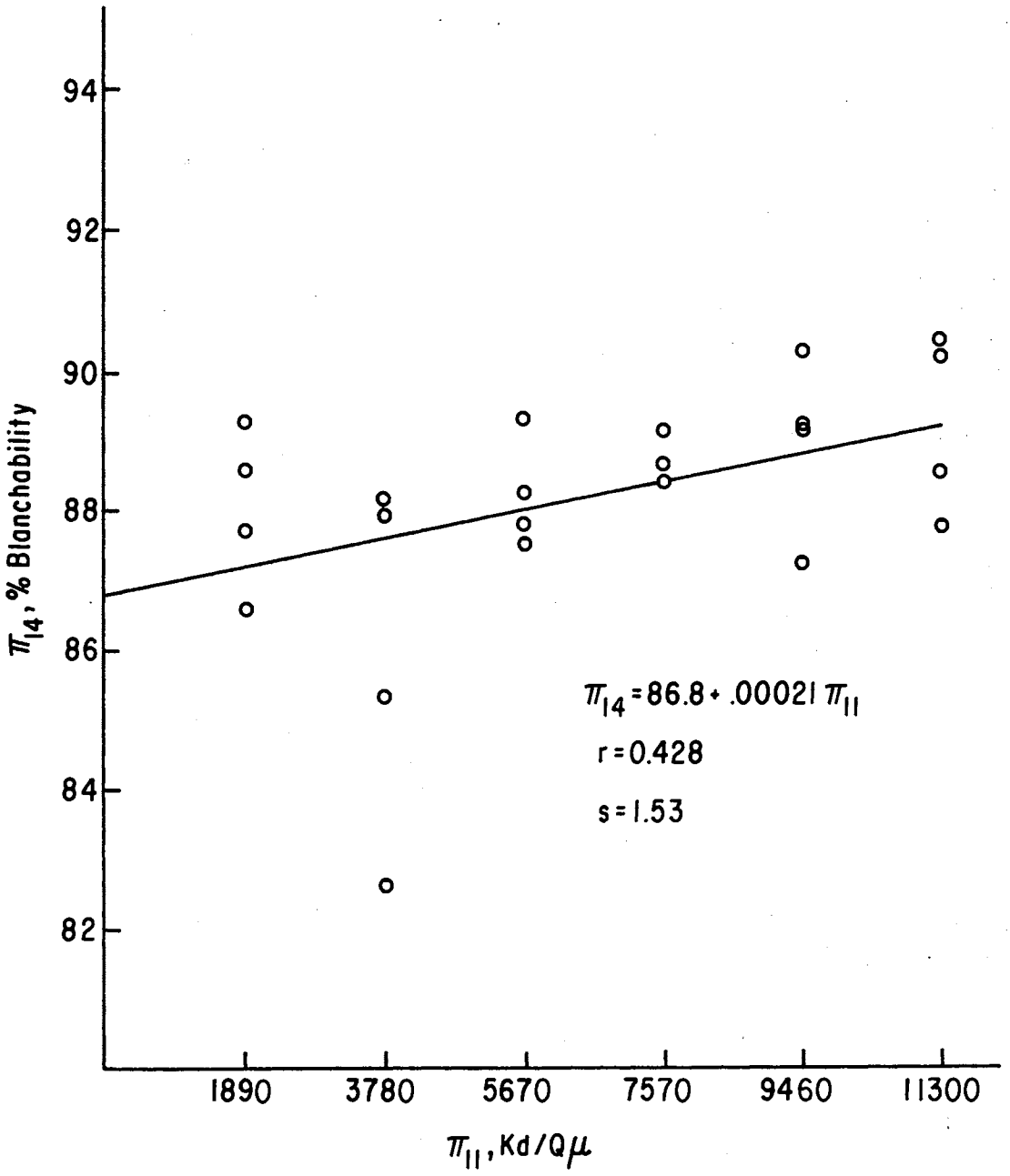

Figure 24. Effects of Blade Force on Blanchability

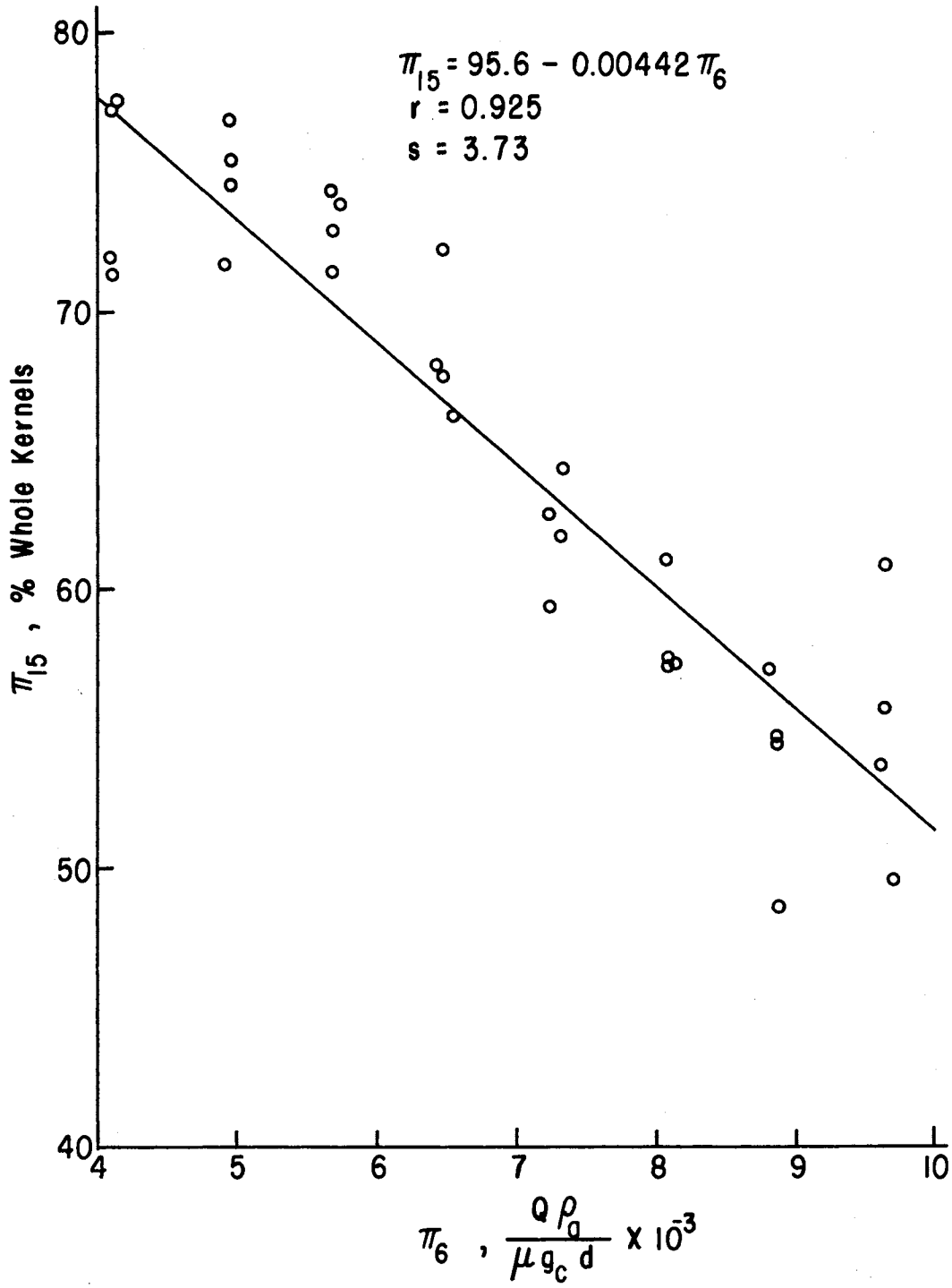

Figure 25. Effects of Reynolds Number on Mechanical Damage

$$F_6\ (\pi_6, \bar{\pi}_9, \bar{\pi}_{11}, \bar{\pi}_{12}) = 95.6 \quad - 0.00442\ \pi_6 \tag{7}$$

Figure 25 shows that as π_6 increases the mechanical damage increases. Therefore, as the air flow of the system increases the mechanical damage to the kernel also increases.

A linear regression analysis shows for π_{11}, blade force, the slope of the regression line is significantly different from zero at the 99% confidence level. Figure 26 shows the effect of π_{11} on mechanical damage. The component equation for blade force is

$$F_{11}(\bar{\pi}_6, \bar{\pi}_9, \pi_{11}, \bar{\pi}_{12}) = \quad 68.0 - 0.000726\ \pi_{11} \tag{8}$$

As force on the blade increases the mechanical damage increases. This result was also observed by Morgan (6).

The effect of π_{12}, blade depth, is significant at the 99.9% confidence level. The component equation for blade depth is

$$F_{12}\ (\bar{\pi}_6, \bar{\pi}_9, \bar{\pi}_{11}, \pi_{12}) = 80.81 - 61.43\ \pi_{12} \tag{9}$$

Figure 27 shows an increase in blade depth results in an increase in mechanical damage.

Figure 28 shows the effect of π_9, initial moisture content, on mechanical damage. Data for both slit and nonslit tests are plotted in Figure 28. The component equation for initial moisture content with slit kernels is

$$F_9\ (\bar{\pi}_6, \pi_9, \bar{\pi}_{11}, \bar{\pi}_{12}) = 73.19 - 1.71\ \pi_9 \tag{10}$$

These tests form a basis for comparison of slitter effectiveness. Analysis shows a decrease in whole kernels in both slit and nonslit samples, as initial moisture content increases. Slitting the testa decreases the whole kernels by about 14.5% at all initial moisture content levels.

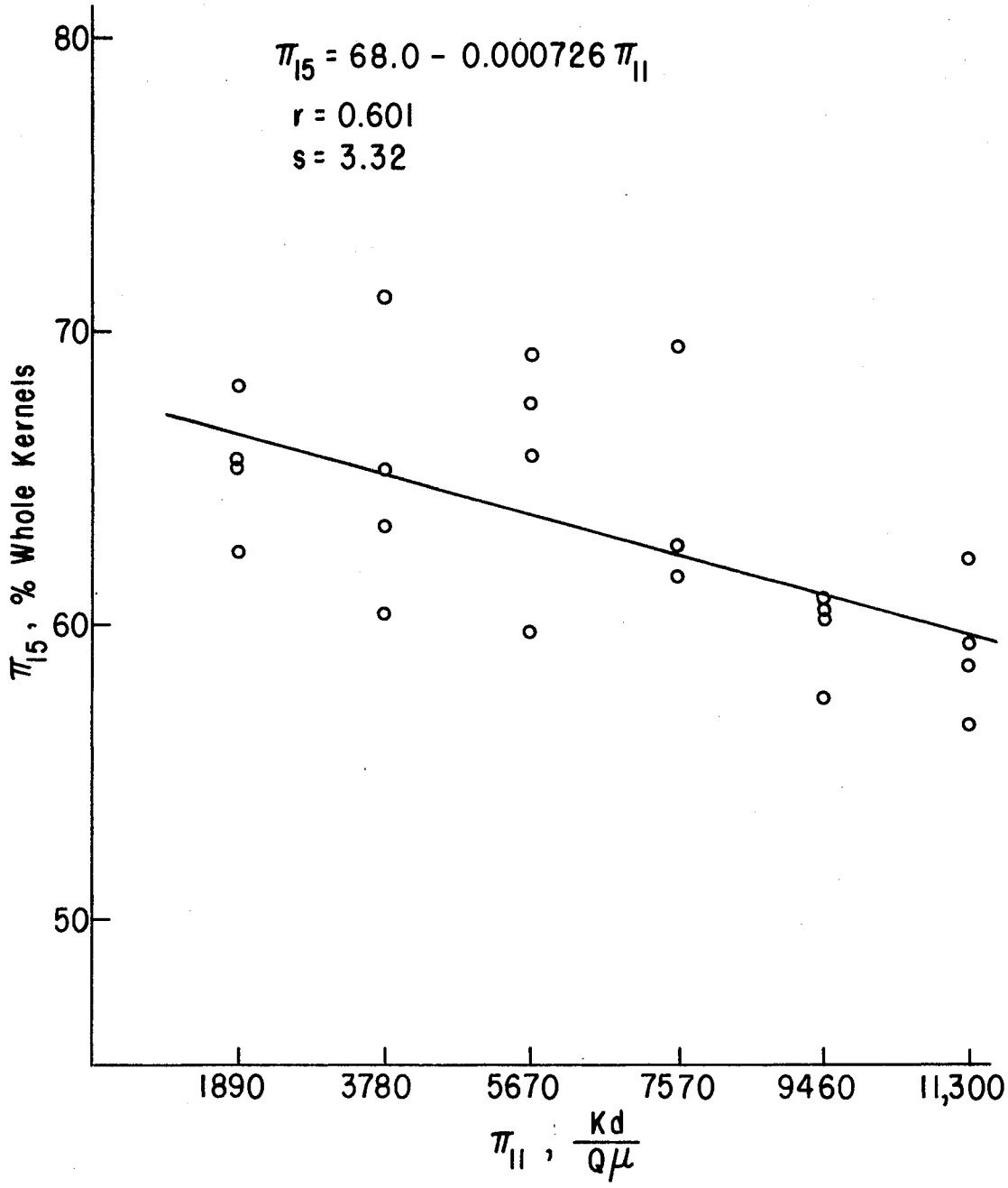

Figure 26. Effects of Blade Force on Mechanical Damage

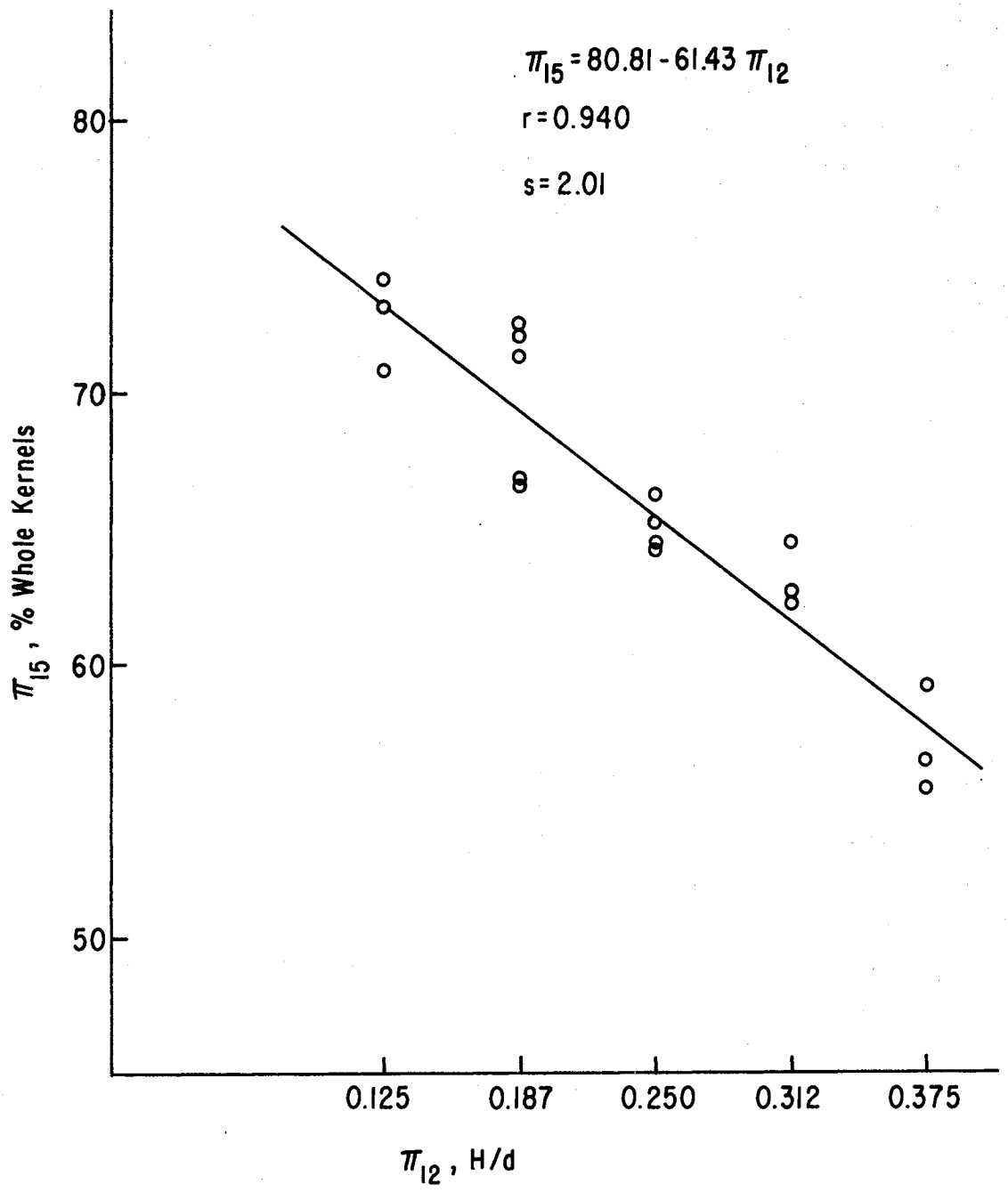

Figure 27. Effects of Blade Depth on Mechanical Damage

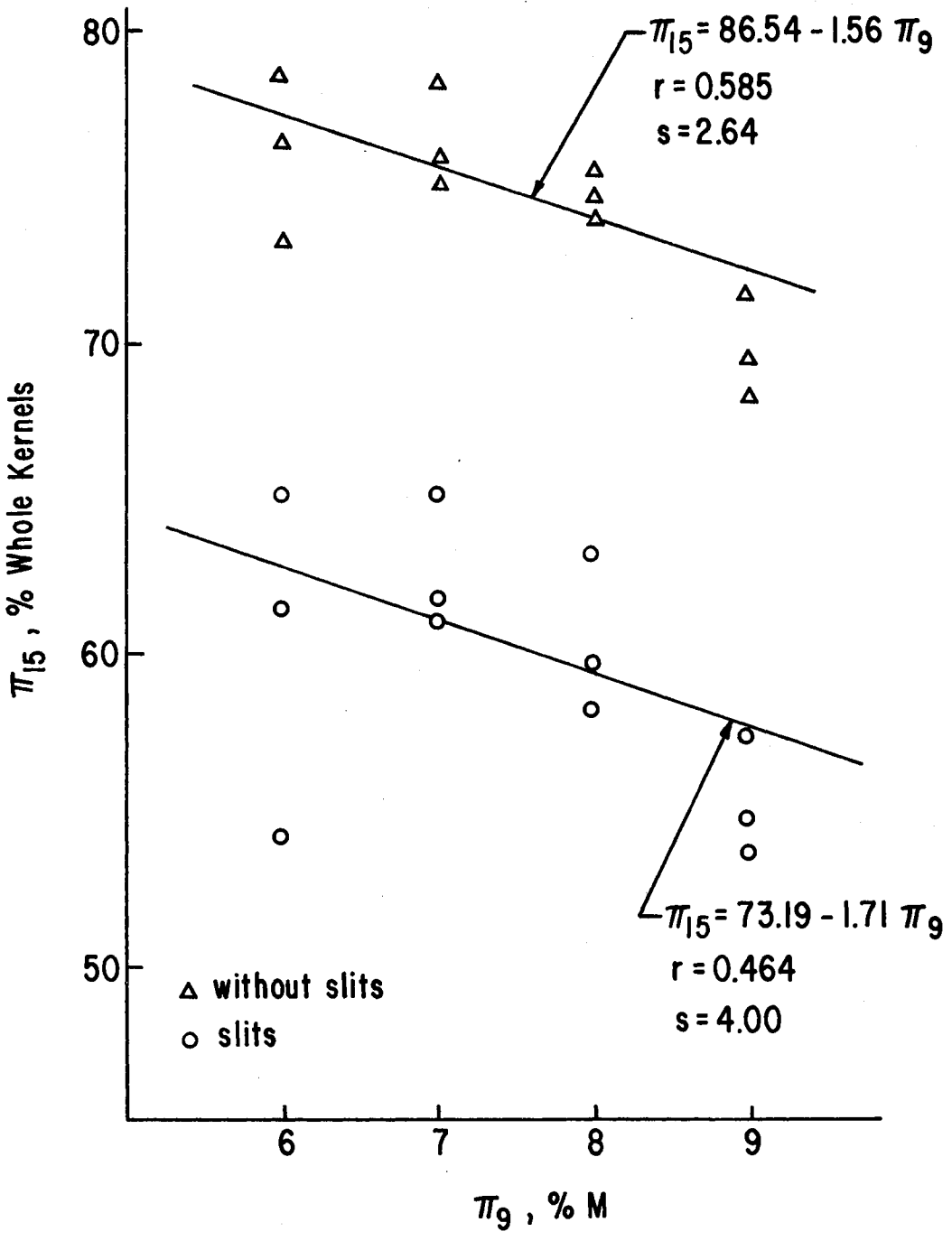

Figure 28. Comparison of Effects of Initial Moisture Content of Both Slit and Nonslit Testa on Mechanical Damage

The results from π_{16}, tube length, and π_7, feeder speed, are plotted in Figure 29 and Figure 30, respectively. Slope of the linear regression lines was shown to be zero for these variables. A horizontal line is drawn through the means of the data points.

As outlined in Chapter III, 15 independent and dimensionless groups, Pi terms, are necessary to adequately describe the pneumatic peanut slitter. Eight of these Pi terms are held constant and six Pi terms are varied.

Three replications of the experimental plan shown in Table III were conducted. One complete replication was finished before another replication was begun. Component equations were developed from these results.

The analysis requires the development of three component equations for π_{14} and four component equations for π_{15}. The component equations for π_{14} are

$$\pi_{14} = f_9 (\pi_9, \bar{\pi}_{11}, \bar{\pi}_{12})$$

$$\pi_{14} = f_{11} (\bar{\pi}_9, \pi_{11}, \bar{\pi}_{12})$$

$$\pi_{14} = f_{12} (\bar{\pi}_9, \bar{\pi}_{11}, \pi_{12})$$

and for π_{15} are

$$\pi_{15} = F_6 (\pi_6, \bar{\pi}_9, \bar{\pi}_{11}, \bar{\pi}_{12})$$

$$\pi_{15} = F_9 (\bar{\pi}_6, \pi_9, \bar{\pi}_{11}, \bar{\pi}_{12})$$

$$\pi_{15} = F_{11} (\bar{\pi}_6, \bar{\pi}_9, \pi_{11}, \bar{\pi}_{12})$$

$$\pi_{15} = F_{12} (\bar{\pi}_6, \bar{\pi}_9, \bar{\pi}_{11}, \pi_{12})$$

The bar over the Pi term indicates the group is held constant throughout the series of tests.

Methods for combining component equations to give the general prediction equations is discussed by Murphy (7). For component

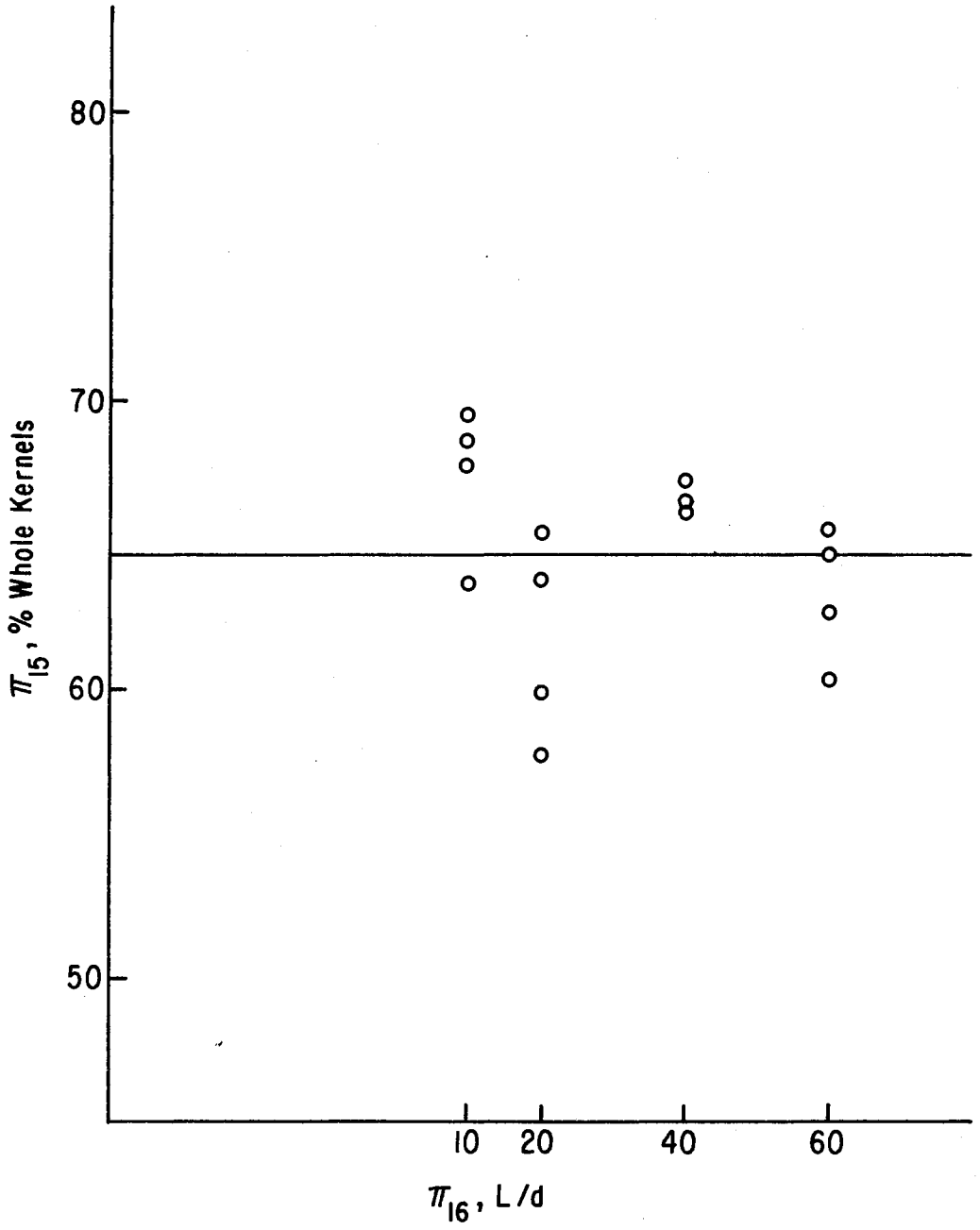

Figure 29. Effects of Tube Length on Mechanical Damage

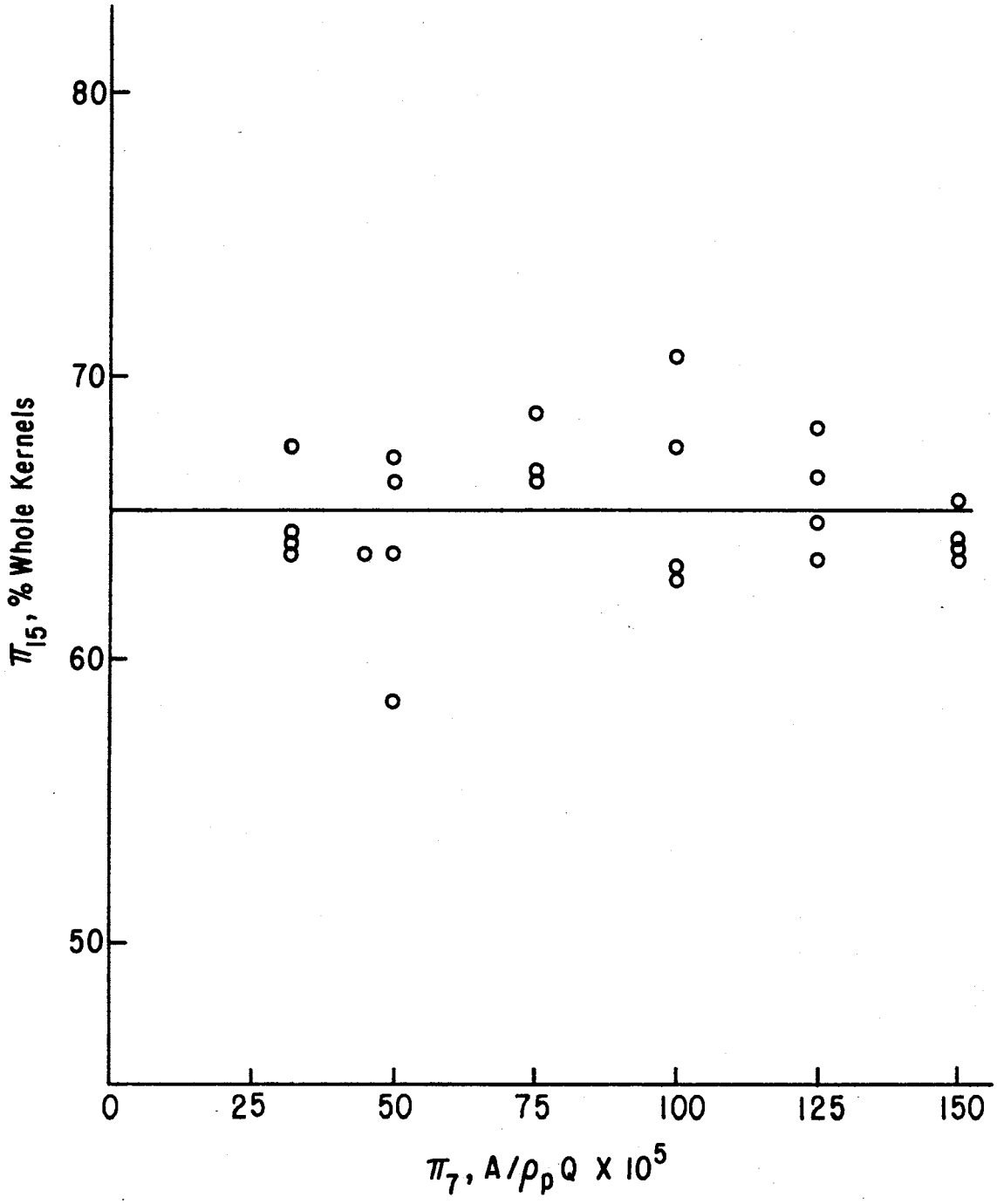

Figure 30. Effects of Feeder Speed on Mechanical Damage

equations that form straight lines on arithmetic coordinates, combination is of the form

$$\pi_{14} = f_9\,(\pi_9, \bar{\pi}_{11}, \bar{\pi}_{12}) + f_{11}\,(\bar{\pi}_9, \pi_{11}, \bar{\pi}_{12}) + f_{12}\,(\bar{\pi}_9, \bar{\pi}_{11}, \pi_{12}) - (n-2)\,f\,(\bar{\pi}_9, \bar{\pi}_{11}, \bar{\pi}_{12}) \quad (11)$$

and

$$\pi_{15} = F_6\,(\pi_6, \bar{\pi}_9, \bar{\pi}_{11}, \bar{\pi}_{12}) + F_9\,(\bar{\pi}_6, \pi_9, \bar{\pi}_{11}, \bar{\pi}_{12}) + F_{11}\,(\bar{\pi}_6\ \bar{\pi}_9\ \pi_{11}\ \bar{\pi}_{12}) + F_{12}\,(\bar{\pi}_6, \bar{\pi}_9, \bar{\pi}_{11}, \pi_{12}) - (n-2)\,F\,(\bar{\pi}_6, \bar{\pi}_9, \bar{\pi}_{11}, \bar{\pi}_{12}) \quad (12)$$

Again the bar over the Pi term indicates the group is held constant throughout the series of tests. The constant values for the Pi terms are

$\bar{\pi}_6 = 7300$ $\qquad$ $\bar{\pi}_{11} = 7566$

$\bar{\pi}_9 = 7.0$ $\qquad$ $\bar{\pi}_{12} = 0.25$

$f\,(\bar{\pi}_9, \bar{\pi}_{11}, \bar{\pi}_{12})$ may be calculated from either equation 4, 5, or 6. The results are

$$f\,(\bar{\pi}_9, \bar{\pi}_{11}, \bar{\pi}_{12}) = 76.32 + 1.82\,\bar{\pi}_9 = 76.32 + 1.82\,(7.0) = 89.06$$

$$f\,(\bar{\pi}_9, \bar{\pi}_{11}, \bar{\pi}_{12}) = 86.8 + 0.00021\,\bar{\pi}_{11} = 86.8 + 0.00021\,(7566) = 88.42$$

$$f\,(\bar{\pi}_9, \bar{\pi}_{11}, \bar{\pi}_{12}) = 83.61 + 15.78\,\bar{\pi}_{12} = 83.61 + 15.78\,(0.25) = 87.55$$

therefore,

$$f\,(\bar{\pi}_9, \bar{\pi}_{11}, \bar{\pi}_{12}) = \frac{89.06 + 88.42 + 87.55}{3} = 88.34$$

Substituting values in Equation 11 yields

$$\pi_{14} = 76.32 + 1.82\ \pi_9 + 86.8\ + 0.00021\ \pi_{11} + 83.61 + 15.78\ \pi_{12} - 176.68$$

After simplifying

$$\pi_{14} = 70.09 + 1.82\ \pi_9 + 0.00021\ \pi_{11} + 15.78\ \pi_{12}$$

or

$$B = 70.09 + 1.82\ (M) + 0.00021 \frac{Kd}{Q\mu} + 15.78\ \frac{H}{d} \qquad (13)$$

$F\ (\overline{\pi}_6, \overline{\pi}_9, \overline{\pi}_{11}, \overline{\pi}_{12})$ may be calculated from either Equation 7, 8, 9, or 10. The results are

$$F\ (\overline{\pi}_6, \overline{\pi}_9, \overline{\pi}_{11}, \overline{\pi}_{12}) = 95.6\ - 0.00442\ \overline{\pi}_6$$
$$= 95.6\ - 0.00442\ (7300) = 63.28$$
$$F\ (\overline{\pi}_6, \overline{\pi}_9, \overline{\pi}_{11}, \overline{\pi}_{12}) = 73.19 - 1.71\ \overline{\pi}_9$$
$$= 73.19 - 1.71\ (7.0) = 61.22$$
$$F\ (\overline{\pi}_6, \overline{\pi}_9, \overline{\pi}_{11}, \overline{\pi}_{12}) = 68.0\ - 0.000726\ \overline{\pi}_{11}$$
$$= 68.0\ - 0.000726\ (7566) = 62.53$$
$$F\ (\overline{\pi}_6, \overline{\pi}_9, \overline{\pi}_{11}, \overline{\pi}_{12}) = 80.81 - 61.43\ \overline{\pi}_{12}$$
$$= 80.81 - 61.43\ (0.25) = 65.45$$

therefore,

$$F\ (\overline{\pi}_6, \overline{\pi}_9, \overline{\pi}_{11}, \overline{\pi}_{12}) = \frac{63.28 + 61.22 + 62.53 + 65.45}{4}$$
$$= 63.12$$

Substituting in values in Equation 12 yields

$$\pi_{15} = 95.6\ - 0.00442\ \pi_6 + 73.19 - 1.71\ \pi_9 + 68.0 - 0.000726\ \pi_{11} + 80.81 - 61.43\ \pi_{12} - 189.36$$

After simplifying

$$\pi_{15} = 128.22 - 0.00442\ \pi_6 - 1.71\ \pi_9 - 0.000726\ \pi_{11} - 61.43\ \pi_{12}$$

or

$$W = 128.22 - 0.00442 \frac{Q\rho_a}{\mu g_c d} - 1.71 (M) - 0.000726 \frac{Kd}{Q\mu} - 61.43 \frac{H}{d} \quad (14)$$

Predicted versus observed results for blanchability and mechanical damage are shown in Figures 31 and 32. The observed blanchability data and mechanical damage data were used to develop the prediction equations. Both of these plots serve to indicate that the component equations have been combined satisfactorily. Extrapolation beyond the limits of the values of the Pi terms used to develop these prediction equations may lead to erroneous results.

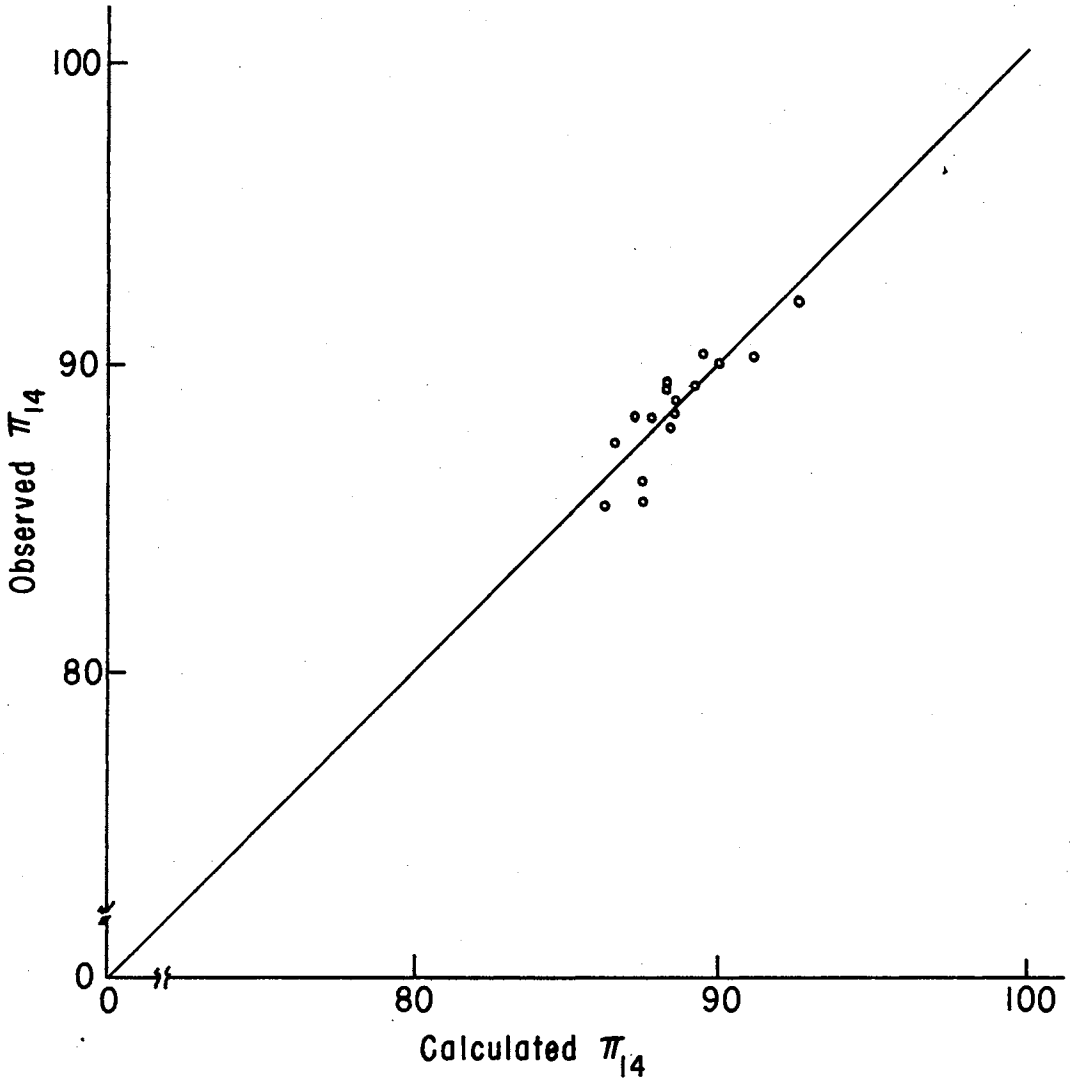

Figure 31. Predicted vs. Observed Blanchability

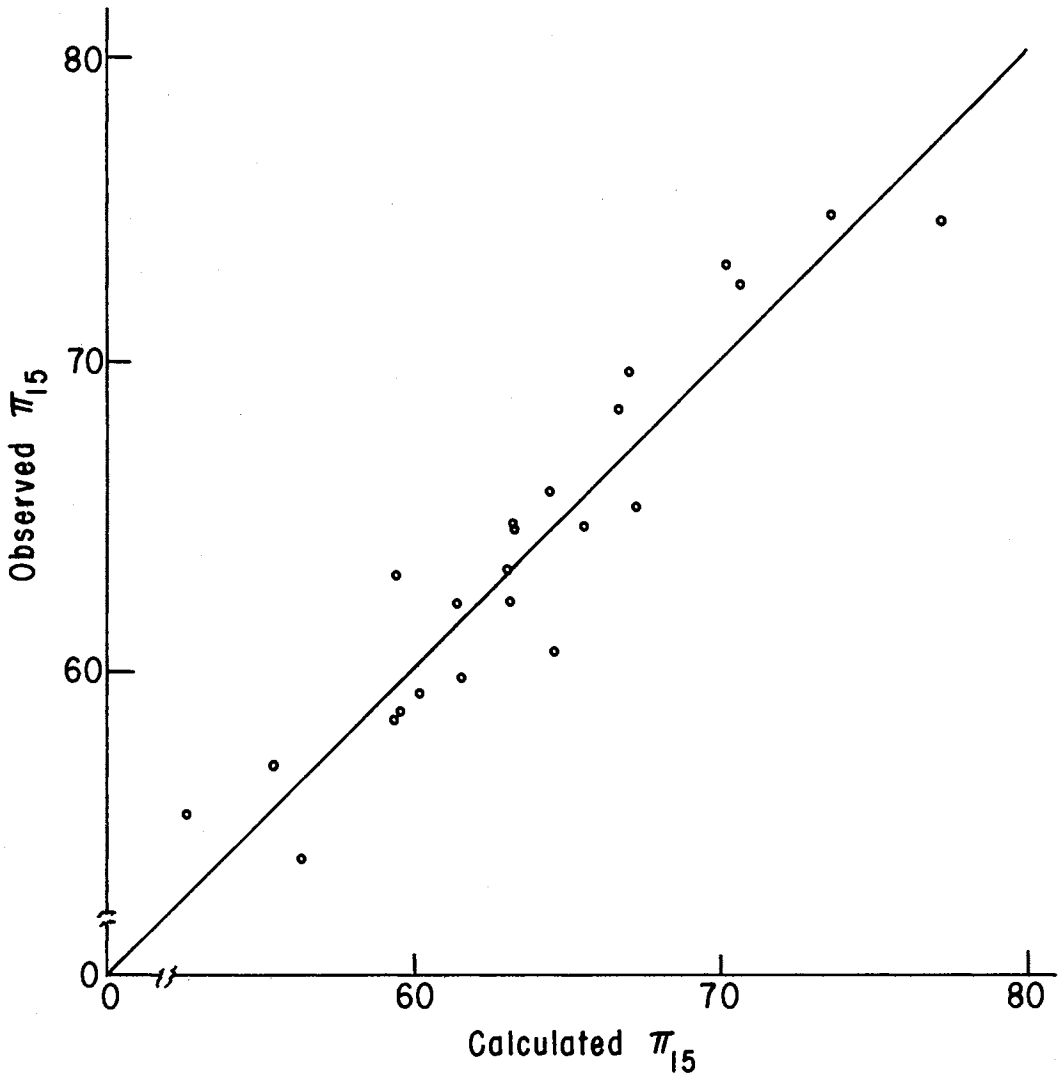

Figure 32. Predicted vs. Observed Mechanical Damage

CHAPTER VI

SUMMARY AND CONCLUSION

Summary

The primary objective of this study was to design, construct, and test a pneumatic peanut skin slitter. A 0.5 throat Coanda nozzle was used as the air conveying device. A 0.5 inch inside diameter plexiglass tube was used as the conveying pipe for the peanut kernels. The slitter block was arranged with three surgical blades mounted 120° apart.

Secondary air flow tests for the four different tube lengths were run with varying primary air flow. Secondary air flow rates were established from this data.

Kernel velocity tests were run to determine the velocity of the kernels with varying primary air flow travelling in a tube two feet long following the Coanda nozzle. From these tests kernel speeds for sized and unsized kernels were established.

A dimensional analysis was done on the variables affecting blanchability and mechanical damage. From the analysis an experimental design was established for testing the effect of these variables on blanchability and mechanical damage.

Employing the methods of similitude, component equations were developed that fitted a straight line on arithmetic coordinates. Combining these component equations by addition yielded the following equations for predicting blanchability and mechanical damage for

Spanish peanut kernels.

$$B = 70.09 + 1.82\ (M) + 0.00021\ \frac{Kd}{Q\mu} + 15.78\ \frac{H}{d} \qquad (13)$$

$$W = 128.22 - 0.00442\ \frac{Q\rho_a}{\mu g_c d} - 1.71\ (M) - 0.000715\ \frac{Kd}{Q\mu} - 61.43\ \frac{H}{d} \qquad (14)$$

Conclusions

The following conclusions are based on the interpretation of the experimental results.

1. Mechanically placing three slits in the peanut testa will improve blanchability of Spanish peanut kernels. The increase in blanchability is more pronounced at 6% initial moisture content than at 9% initial moisture content.
2. An increase in kernel mechanical damage due to slitting the kernels is observed at all initial moisture content levels.
3. Increasing the Reynolds number had no effect on blanchability, however increases in mechanical damage were observed as Reynolds number increased.
4. Feeder speed had no effect on the blanchability or mechanical damage.
5. Tube length between nozzle and slitter has no effect on blanchability or mechanical damage.
6. Increasing blade force results in both increased blanchability and increased mechanical damage.
7. Increasing blade depth increases blanchability and mechanical damage.
8. When an increase in blanchability was observed from a variable

increase in mechanical damage was also observed.

SELECTED BIBLIOGRAPHY

(1) "Analysis of Thrust Due to Coanda Phenomenon." SFERI-Coanda (Clichy, France) AFOSR REPORT on Contract AF 61(052) 382, Oct. 1960.

(2) Barnes, P. C. Jr., Charles E. Holaday, and Jack L. Pearson. "Device to Measure Ease of Skin Removal from Peanuts." Journal of Food Science, Vol. 36 (1971), pp. 405-407.

(3) Henderson, S. M. and R. L. Perry. Agricultural Process Engineering. New York: John Wiley & Sons, Inc., 1966.

(4) Lawler, F. K. "Ingenuity Creates New Process." Food Engr., Vol. 33, No. 2 (1961), p. 38.

(5) Marks, L. S. Mechanical Engineers Handbook. New York: McGraw-Hill Book Company, Inc., 1951.

(6) Morgan, R. G. "Improved Blanching of Raw Spanish Peanuts." (Unpub. Report, Oklahoma State University, 1973).

(7) Murphy, Glenn. Similitude in Engineering. New York: The Ronald Press Co., 1950.

(8) Pominski, J., E. L. D'Aquin, L. J. Molaison, E. J. McCourtney, and H. L. E. Vix. "Pre-treatment of Peanut Kernels for Effective Skin Removal." J. Am. Oil Chemists Soc., Vol. 29, No. 2 (1952), pp. 48-51.

(9) Reba, Imants. "Applications of the Coanda Effect." Scientific American, Vol. 214, No. 6 (1966), pp. 84-92.

(10) Reba, Imants. "A Preliminary Study of the Coanda Nozzle Principle for Propulsion of Tube Vehicles." Report IITRI J 6128, 1968.

(11) Reeve, K. J. "Split Skins Spun Off in New Nut Blancher." Food Engr., Vol. 34, No. 8 (1962), p. 51.

(12) Shackelford, P. S., B. L. Clary, G. H. Brusewitz, G. V. Odell, and J. Pominski. "Skin Removal from Spanish Peanuts by Heating to Moderate Temperatures." ASAE Paper No. 72-893, American Society of Agricultural Engineers, St. Joseph, Michigan, 1972.

(13) Victory, E. L. "Analysis of Thrust and Flow Augmentation of a Coanda Nozzle." Report ARL, 1965, pp. 65-86.

(14) Wetmore, Alan Curtis. "Evaluation of a Coanda Nozzle for Pneumatic Conveying." (Unpub. M. S. Thesis, Oklahoma State University, 1972)

APPENDIX A

WORKING DRAWINGS OF

COANDA NOZZLE

APPENDIX A-I

COANDA NOZZLE SURFACE SECTION

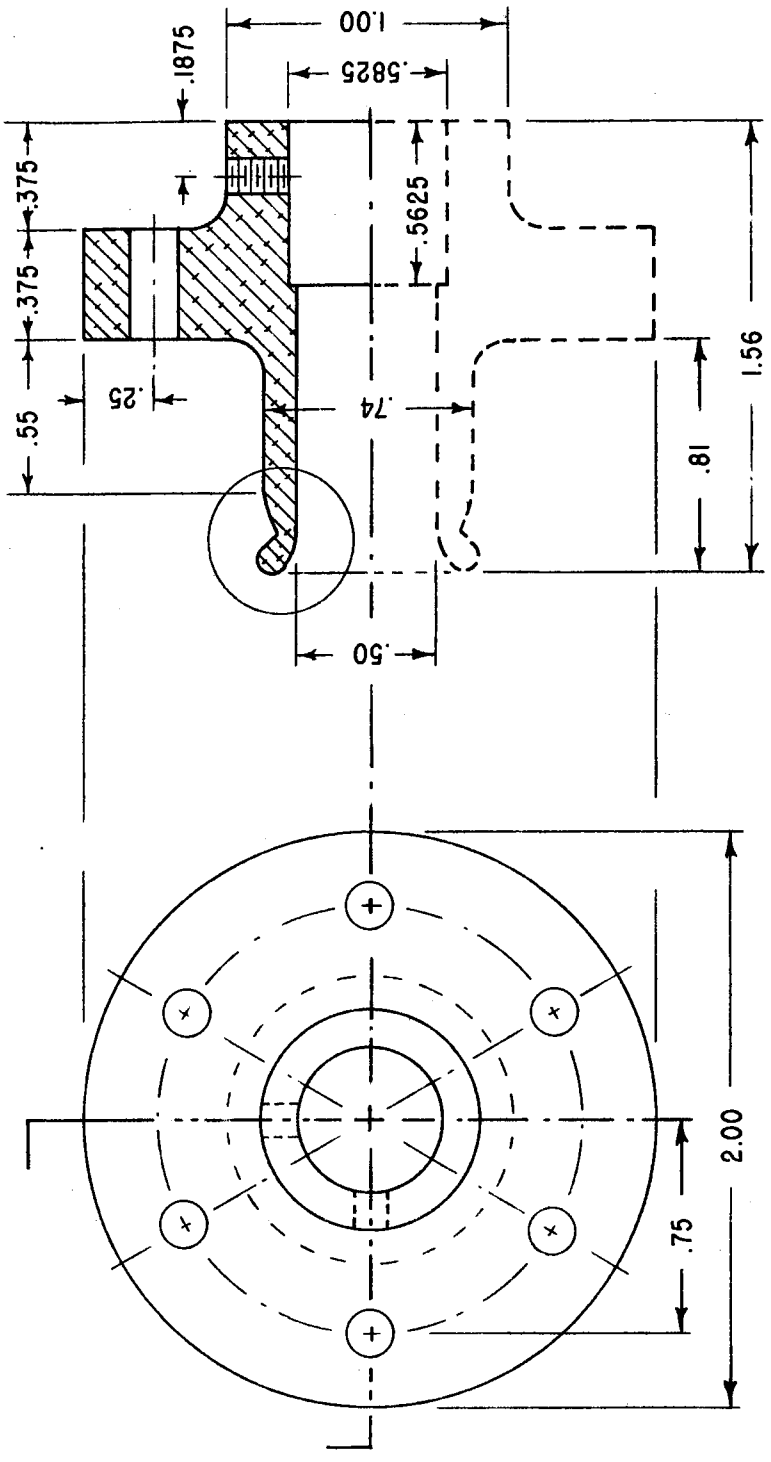

Dimensions are in inches.

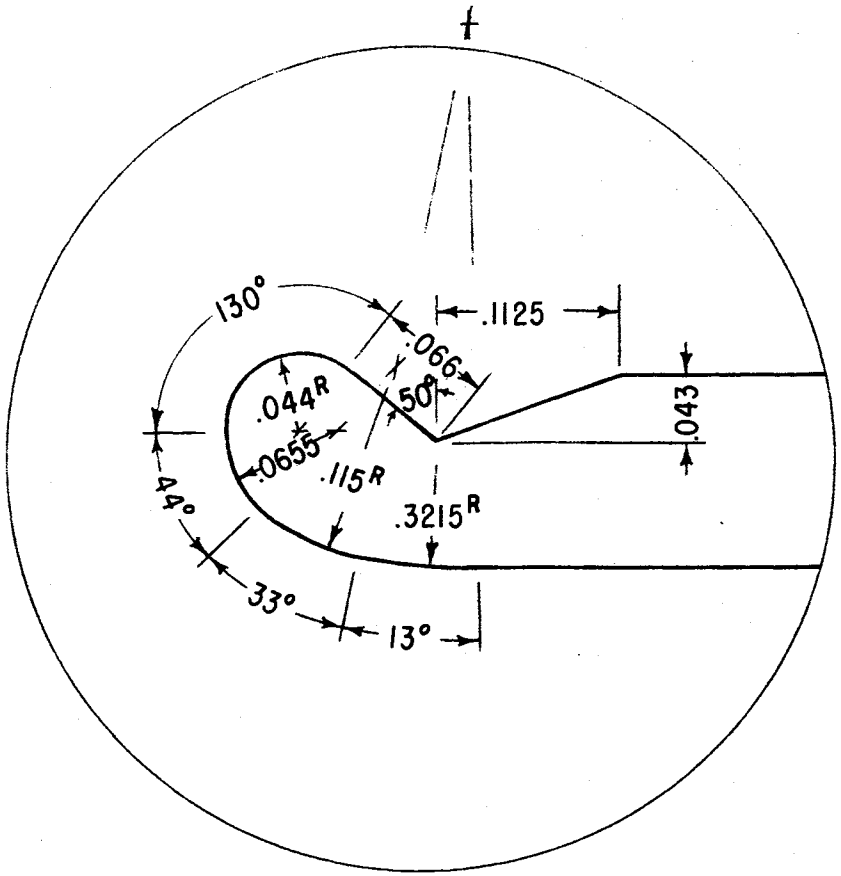

APPENDIX A-II

COANDA SURFACE DETAIL

Dimensions are in inches.

APPENDIX A-III

COANDA NOZZLE WALL SECTION

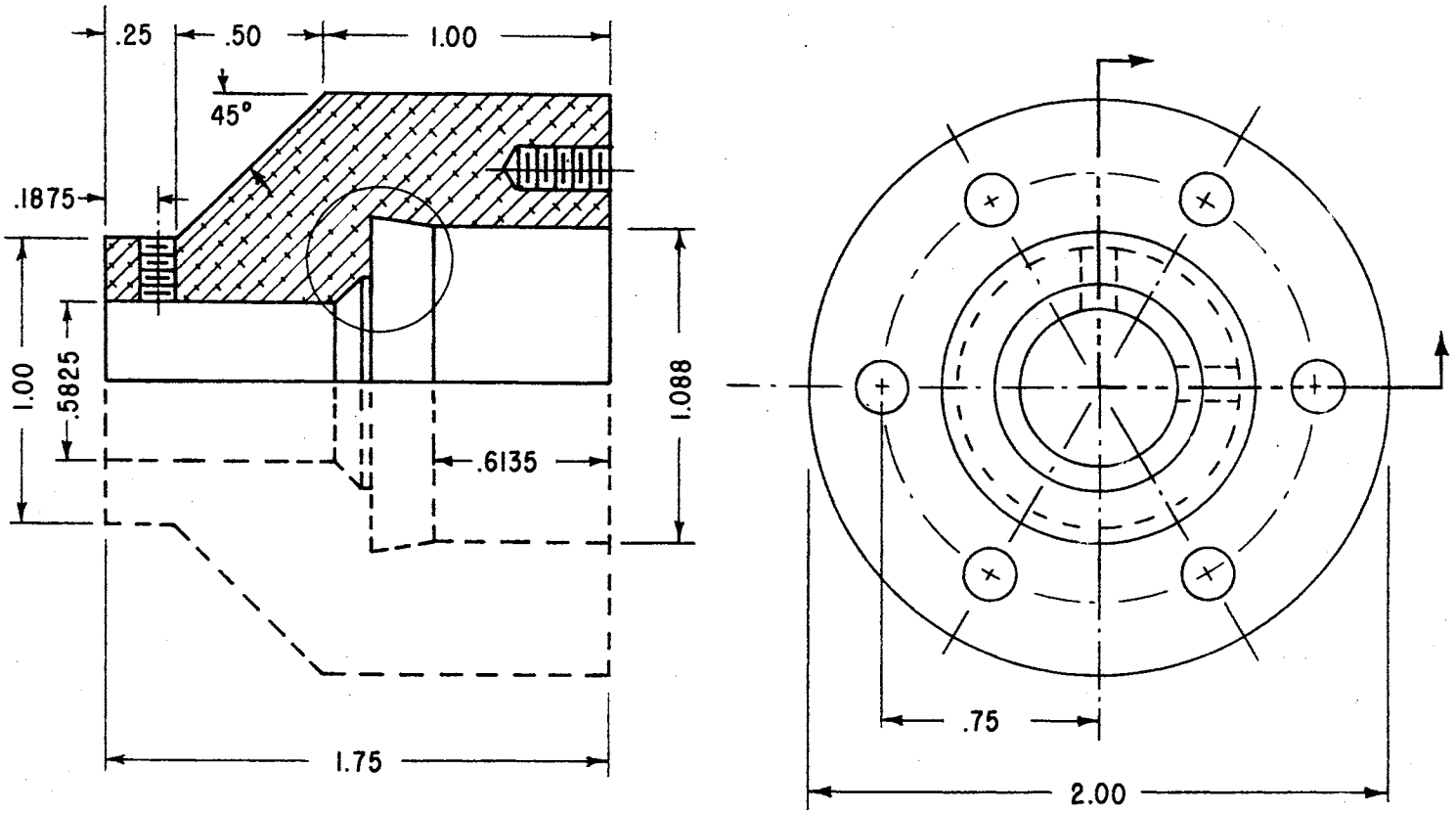

Dimensions are in inches.

APPENDIX A-IV

COANDA NOZZLE WALL DETAIL

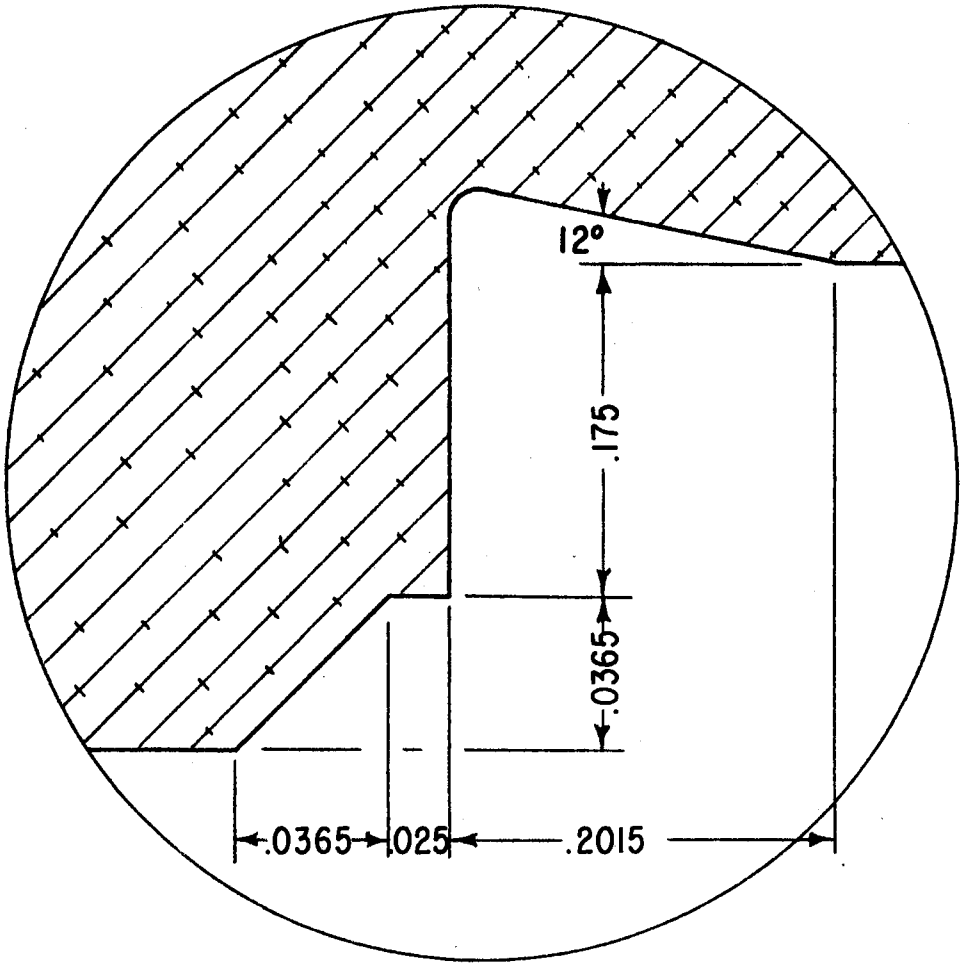

Dimensions are in inches.

APPENDIX B

WORKING DRAWINGS OF

SLITTER BLOCK

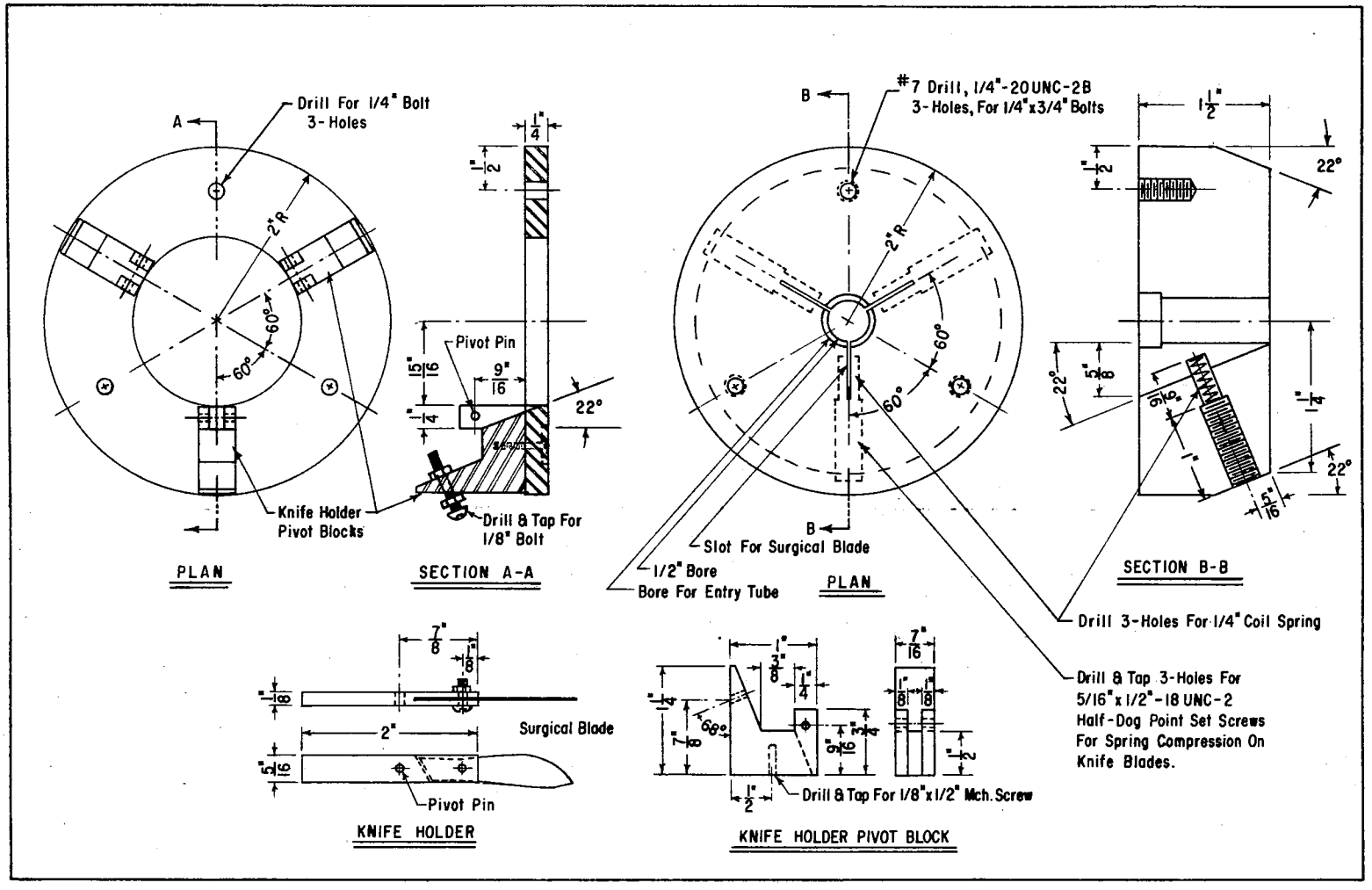

APPENDIX B-1

SLITTER BLOCK DESIGN

APPENDIX C

PNEUMATIC PEANUT SKIN SLITTER DATA

APPENDIX C-I

DATA FOR ROTAMETER CALIBRATION

Scale Reading	CFM	Scale Reading	CFM
0.10	2.154	1.00	16.632
0.15	3.047	1.05	17.178
0.20	3.732	0.10	3.036
0.25	4.309	0.15	3.036
0.30	5.278	0.20	3.719
0.35	6.094	0.25	4.801
0.40	6.814	0.30	5.259
0.45	7.769	0.35	6.441
0.50	8.619	0.40	6.790
0.55	9.142	0.45	7.742
0.60	10.107	0.50	8.034
0.65	11.197	0.55	9.110
0.70	11.802	0.60	9.840
0.75	12.565	0.65	10.736
0.80	13.457	0.70	11.761
0.85	14.455	0.75	12.520
0.90	15.084	0.80	13.236
0.95	15.835	0.85	14.243
1.00	16.411	0.90	15.183
1.05	17.373	0.10	1.673
1.10	18.029	0.15	2.646
0.10	2.147	0.20	3.416
0.15	3.036	0.25	4.322
0.20	3.719	0.30	5.293
0.25	4.294	0.35	6.112
0.30	5.259	0.40	6.833
0.35	6.073	0.45	8.085
0.40	6.790	0.50	8.644
0.45	7.742	0.55	9.419
0.50	8.316	0.60	10.136
0.55	9.359	0.65	11.019
0.60	10.071	0.70	11.836
0.65	10.949	0.75	12.601
0.70	11.761	0.80	13.321
0.75	12.703	0.85	14.170
0.80	13.236	0.90	15.280
0.85	13.915	0.95	15.880
0.90	15.030	1.00	16.599

APPENDIX C-II

KERNEL SPEED DATA WITH SIZED PEANUTS

Reynolds No.	Kernel Speed (ft/sec)	Reynolds No.	Kernel Speed (ft/sec)
4126	22.22	7295	42.55
4126	17.85	7295	50.00
4126	21.27	7295	41.66
4126	18.86	7295	55.55
4126	20.83	7295	47.61
4126	18.51	8087	47.61
4918	28.16	8087	45.45
4918	25.31	8087	55.55
4918	24.69	8087	52.63
4918	27.02	8087	52.63
4918	28.16	8087	55.55
4918	26.31	8087	58.82
5710	32.25	8087	50.00
5710	32.78	8879	37.73
5710	32.25	8879	64.51
5710	28.57	8879	66.66
5710	30.30	8879	52.63
5710	37.03	8879	50.00
5710	32.78	8879	50.00
6502	38.46	8879	66.66
6502	37.73	8879	62.50
6502	40.81	8879	55.55
6502	37.03	8879	60.60
6502	44.44	8879	62.50
6502	41.66	9658	46.51
6502	36.36	9658	35.71
6502	45.45	9658	62.50
6502	35.71	9658	64.51
7295	41.66	9658	50.00
7295	47.61	9658	62.50
7295	43.47	9658	38.46

APPENDIX C-III

KERNEL SPEED DATA WITH UNSIZED PEANUTS

Reynolds No.	Kernel Speed (ft/sec)	Reynolds No.	Kernel Speed (ft/sec)
4111	13.69	7269	43.47
4111	16.80	7269	41.66
4111	15.62	7269	40.00
4111	16.12	7269	41.66
4111	13.69	8058	43.47
4900	24.69	8058	47.61
4900	23.25	8058	47.61
4900	22.98	8058	48.78
4900	23.80	8058	45.45
4900	23.25	8058	40.00
4900	26.31	8058	51.58
4900	27.77	8848	50.00
5690	31.25	8848	55.55
5690	28.98	8848	45.45
5690	27.77	8848	58.82
5690	30.30	8848	50.00
5690	30.30	8848	54.05
6579	35.08	8848	52.63
6479	36.36	9637	60.60
6479	32.35	9637	66.66
6479	36.36	9637	62.50
6479	34.48	9637	55.55
6479	36.36	9637	60.60
7269	43.47	9637	58.82
7269	45.45	9637	60.60
7269	44.44	9637	43.47
7269	39.21	9637	68.96
7269	37.03	9637	62.50

APPENDIX C-IV

SECONDARY AIR FLOW RATE DATA FOR DIFFERENT LENGTH TUBES

Scale Reading	5 Inch Tube CFM	10 Inch Tube CFM	20 Inch Tube CFM	30 Inch Tube CFM
0.100	4.563	3.670	3.130	3.130
0.125	5.960	5.071	4.427	4.427
0.150	7.086	6.062	5.308	5.308
0.175	8.784	7.257	6.358	6.822
0.200	10.083	8.573	7.257	7.747
0.225	12.073	9.961	8.644	8.991
0.250	13.327	11.067	9.837	10.022
0.275	14.849	12.521	10.956	11.287
0.300		13.600	11.765	
0.100	4.824	3.670	3.130	3.130
0.125	6.162	5.071	4.563	4.563
0.150	7.587	6.062	5.534	5.534
0.175	8.923	7.341	6.547	6.911
0.200	10.323	8.429	7.587	7.668
0.225	11.869	9.774	8.644	9.126
0.250	13.142	10.956	9.899	10.204
0.275	14.972	12.521	10.956	11.232
0.300		13.555		
0.100	4.563	3.670	3.323	3.130
0.125	5.751	5.071	4.290	4.824
0.150	7.086	6.358	5.312	5.751
0.175	8.501	7.668	6.067	7.086
0.200	9.961	8.573	7.005	8.133
0.225	11.555	10.143	8.215	9.260
0.250	12.667	11.287	9.333	10.264
0.275	14.043	12.954	10.624	10.844
0.300			11.458	
0.100	4.567	4.290	2.930	2.928
0.125	5.965	5.076	4.290	4.141
0.150	7.092	6.167	5.312	5.308
0.175	8.363	7.347	6.363	6.062
0.200	9.907	8.436	7.092	7.257
0.225	11.564	9.907	8.064	8.501
0.250	12.870	11.077	9.201	9.456
0.275	14.314	12.581	10.624	10.143
0.300			11.458	

APPENDIX C-V

DATA FOR BLANCHABILITY AND MECHANICAL DAMAGE DUE TO π_6, REYNOLDS NUMBER

Run No.	π_6	Blanchability	Mechanical Damage
1	4101	88.06	72.00
101	4115	85.55	77.15
201	4153	88.27	77.52
301	4123	84.85	71.38
2	5692	87.97	74.23
102	5696	86.13	71.37
202	5767	86.00	73.93
302	5707	82.69	72.97
3	7251	86.70	62.85
103	7254	87.12	59.39
203	7367	90.42	64.37
303	7295	93.17	61.97
4	8880	91.07	48.65
104	8857	85.85	54.76
204	8817	91.36	57.18
304	8874	82.49	54.57
5	6482	87.02	72.14
105	6466	90.44	68.09
205	6554	87.74	66.09
305	6484	90.71	67.71
6	8093	87.39	57.26
106	8075	90.69	61.06
206	8151	86.25	57.14
306	8088	88.77	57.42
7	9641	89.19	56.78
107	9617	90.95	53.87
207	9604	87.63	60.88
307	9687	86.30	49.36
8	4953	88.80	76.97
108	4906	88.28	72.75
208	4979	88.46	75.45
308	4955	88.60	74.79

APPENDIX C-VI

DATA FOR BLANCHABILITY AND MECHANICAL DAMAGE DUE TO π_7, FEEDER SPEED

Run No.	π_7	Blanchability	Mechanical Damage
9	0.00031815	89.82	63.74
109	0.00031815	88.38	63.92
209	0.00031815	88.41	67.58
309	0.00031815	88.56	64.37
10	0.00050905	89.81	58.40
110	0.00050905	89.01	63.64
210	0.00050905	87.34	66.16
310	0.00050905	82.38	67.06
11	0.00076357	87.23	68.82
111	0.00076357	88.55	66.13
211	0.00076357	86.91	66.58
12	0.00101810	87.84	63.26
112	0.00101810	88.36	62.90
212	0.00101810	89.25	67.42
312	0.00101810	88.14	70.68
13	0.00127262	87.75	64.96
113	0.00127262	90.10	63.60
213	0.00127262	87.17	66.34
313	0.00127262	87.99	68.01
14	0.00152715	89.25	64.14
114	0.00152715	86.53	65.62
214	0.00152715	87.44	63.53
314	0.00152715	88.99	63.82

APPENDIX C-VII

DATA FOR BLANCHABILITY AND MECHANICAL DAMAGE DUE TO π_9, INITIAL MOISTURE

Run No.	π_9	Blanchability	Mechanical Damage
21	6	89.92	54.31
121	6	86.50	65.47
221	6	86.20	61.97
22	7	88.95	62.19
122	7	87.38	61.80
222	7	89.25	65.89
23	8	90.03	63.42
123	8	92.83	59.69
223	8	90.70	63.10
24	9	92.03	57.48
124	9	93.61	53.74
224	9	92.55	54.56

APPENDIX C-VIII

DATA FOR BLANCHABILITY AND MECHANICAL DAMAGE DUE TO NOT SLITTING THE TESTA

Run No.	Initial Moisture	Blanchability	Mechanical Damage
6NS1	6	82.50	76.41
6NS2	6	82.42	73.37
6NS3	6	83.59	78.83
7NS1	7	82.58	75.45
7NS2	7	83.80	75.85
7NS3	7	86.28	78.63
8NS1	8	90.07	74.84
8NS2	8	89.94	75.44
8NS3	8	89.28	74.06
9NS1	9	92.06	76.60
9NS2	9	91.66	68.44
9NS3	9	89.46	69.78

APPENDIX C-IX

DATA FOR BLANCHABILITY AND MECHANICAL DAMAGE DUE TO π_{11}, BLADE FORCE

Run No.	π_{11}	Blanchability	Mechanical Damage
15	1891.6	89.25	62.64
115	1891.6	87.88	65.32
215	1891.6	86.79	68.10
315	1891.6	88.78	65.39
16	3783.2	87.96	65.36
116	3783.2	82.73	71.09
216	3783.2	88.18	60.19
316	3783.2	85.30	63.28
17	5674.8	89.36	59.92
117	5674.8	88.28	67.51
217	5674.8	87.59	69.19
317	5674.8	87.75	66.82
18	7566.4	88.79	61.77
118	7566.4	89.08	62.85
218	7566.4	88.54	69.52
19	9458.0	89.13	60.41
119	9458.0	89.08	60.38
219	9458.0	90.26	57.50
319	9458.0	87.10	60.92
20	11349.6	90.38	56.67
120	11349.6	87.79	62.22
220	11349.6	88.43	59.19
320	11349.6	90.11	58.66

APPENDIX C-X

DATA FOR BLANCHABILITY AND MECHANICAL DAMAGE DUE TO π_{12}, BLADE DEPTH

Run No.	π_{12}	Blanchability	Mechanical Damage
25	0.375	88.61	59.03
125	0.375	90.10	55.39
225	0.375	89.57	56.42
26	0.312	87.05	64.52
126	0.312	86.32	62.19
226	0.312	91.63	62.48
27	0.250	87.38	65.01
127	0.250	85.58	64.62
227	0.250	90.94	64.48
28	0.187	83.76	72.00
128	0.187	81.53	72.32
228	0.187	88.32	71.15
328	0.187	92.05	66.48
428	0.187	88.02	66.59
29	0.125	82.99	73.11
129	0.125	86.11	70.95
229	0.125	86.61	74.01

APPENDIX C-XI

DATA FOR BLANCHABILITY AND MECHANICAL DAMAGE DUE TO π_{16}, TUBE LENGTH

Run No.	π_{16}	Blanchability	Mechanical Damage
30	10	86.96	63.80
130	10	87.68	67.86
230	10	89.29	69.45
330	10	90.27	68.50
31	20	91.02	57.86
131	20	90.21	63.98
231	20	87.67	65.30
331	20	87.66	59.94
32	40	89.59	66.49
132	40	91.15	66.12
232	40	88.52	67.04
33	60	87.16	65.47
133	60	90.17	64.73
233	60	88.88	60.03
333	60	90.23	62.63

VITA

Bethel Joe Herrold

Candidate for the Degree of

Master of Science

Thesis: PNEUMATIC PEANUT SKIN SLITTER

Major Field: Agricultural Engineering

Biographical:

Personal Data: Born in Oklahoma City, Oklahoma, August 8, 1947, the son of Bethel George and Annie Herrold; married to Margie Page on December 30, 1969; father of JoDawna Ann, who was born July 11, 1972.

Education: Graduated from Luther High School, Luther, Oklahoma, in 1965; received the degree of Bachelor of Science in Agricultural Engineering from Oklahoma State University in 1970; completed requirements for the Master of Science degree from Oklahoma State University in May, 1974.

Professional Experience: Graduate Research Assistant, Oklahoma State University from August 1972 to May 1974.

Professional Organizations: Member of the American Society of Agricultural Engineers.